PARIJS

O R S A Y

N° d'ordre : 1476

Sujet de la Thèse :

DETERMINATION EXPERIMENTALE DES SECTIONS EFFICACES DIFFERENTIELLES D'INTERACTIONS DE ν_μ ET $\bar{\nu}_\mu$

Article Principal :

EXPERIMENTAL STUDY OF STRUCTURE FUNCTIONS AND SUM RULES IN CHARGE-CHANGING INTERACTIONS OF NEUTRINOS AND ANTINEUTRINOS ON NUCLEONS

recouvrant en partie la thèse de Doctorat ès Sciences, enregistrée au C.N.R.S., sous le Numéro AO 11732.

Anne-Marie LUTZ née BURBAN

Soutenue le 12 Mai 1975 à l'UNIVERSITE PARIS-SUD, Centre d'Orsay devant le jury :

MM.	J. HAISSINSKI	Président
	P. LEHMANN)	Examinateurs
	M. GOURDIN)	
	A. ROUSSET)	
	B. AUBERT)	

UNIV.
LEIDEN
BIBL.

Jury proposé

MM. J. HAISSINSKI Président

P. LEHMANN

M. GOURDIN

A. ROUSSET

B. AUBERT

RESUME DE LA THESE DE DOCTORAT D'ETAT

présentée par *Anne-Marie LUTZ*

Maître ès Sciences Physiques

Thèse préparée au Laboratoire de l'Accélérateur Linéaire sous la direction de Monsieur B. AUBERT

DETERMINATION EXPERIMENTALE DES SECTIONS EFFICACES DIFFERENTIELLES D'INTERACTIONS DE ν_μ *et* $\bar{\nu}_\mu$

Le but de ce travail est de déterminer les sections efficaces différentielles d'interactions de ν_μ et $\bar{\nu}_\mu$ des types :

$$\nu_\mu N \to \mu^- X \qquad\qquad \bar{\nu}_\mu N \to \mu^+ X$$

où N représente un nucléon, p ou n ;

X représente tout système hadronique.

Les résultats que nous présentons sont déduits de l'analyse de clichés de la grande chambre à bulle Gargamelle de CERN. Remplie de fréon lourd CF_3Br, celle-ci est placée dans un faisceau de ν_μ ou $\bar{\nu}_\mu$ d'énergie comprise entre .5 et 18 GeV environ ($< E_\nu > \sim 2.5$ GeV).

Des rappels relativement brefs sur les conditions générales de l'expérience , les caractéristiques du faisceau, la mesure du flux de ν et les techniques de reconstruction de traces forment le sujet de la première partie de ce travail.

La seconde partie décrit les méthodes utilisées pour résoudre les difficultés essentielles de la détermination des sections efficaces différentielles :

$$\frac{d\sigma^{\nu,\bar{\nu}}}{dx} \quad \text{et} \quad \frac{d\sigma^{\nu,\bar{\nu}}}{dy}$$

$$x \equiv \frac{q^2}{2M\nu} \equiv \frac{E_\mu \left(E_\mu + \nu\right) \left(1 - \cos\theta\right)}{M\nu}$$

$$y \equiv \frac{\nu}{E} = \frac{\nu}{E_\mu + \nu}$$

(où E_μ , ν et θ sont les énergies du μ , de la gerbe hadronique et l'angle entre le μ et le ν , mesurées dans le laboratoire).

Ce sont :

i) l'identification du muon,

ii) la détermination de l'énergie de la gerbe hadronique X.

Le faisceau ν n'est pas monochromatique : l'énergie du ν qui a provoqué une interaction ne peut donc être déduite que de la mesure de l'énergie des traces chargées observées et de l'estimation de l'énergie emportée par les neutres (neutrons ou gammas) détectés ou non. Toute reconstruction cinématique de l'événement est interdite par les réinteractions nucléaires et le moment de Fermi à l'intérieur des noyaux lourds du fréon (CF_3Br) qui remplit la chambre.

1. Ambiguïtés

L'identification du μ ainsi que la mesure de l'énergie des traces chargées requièrent que soit reconnue la nature des particules : en effet la reconstruction géométrique de l'événement ne permet de connaître que l'impulsion et le signe de la trace par sa courbure dans le champ magnétique où est plongée Gargamelle.

La topologie des traces chargées et leur signe permettent de réduire les ambiguïtés mais non pas de les lever toutes :

- une trace positive interagissante pourra signer un π^+ ou p,
- une trace positive qui sort de la chambre pourra signer un μ^+, π^+ ou p ,
- une trace négative qui sort de la chambre pourra signer un μ^- ou π^- .

(Nous négligeons d'autres possibilités que μ, π ou p ; les particules étranges chargées (K^+), sont reconnues lors d'une sélection spéciale des événements).

i) Grâce aux grandes dimensions de la chambre par rapport à la longueur d'interaction des $\pi^\pm$ et p ($\sim$ 70 cm), les hadrons peuvent être bien distingués des μ parmi les traces présentant l'ambiguïté μ/hadron. Celle-ci est résolue par une méthode de pondération où sont calculées, pour les événements présentant plusieurs candidats μ possibles, les probabilités pour chaque trace ambiguë d'être le μ de

l'événement. La trace choisie comme μ (avec une probabilité supérieure à 90 %) est dans 80 % des cas, la trace du signe correspondant au faisceau (μ^- dans les ν_μ , μ^+ dans les $\bar{\nu}_\mu$) qui a l'impulsion maximum. Ceci est dû à la grande longueur potentielle de ces traces émises préférentiellement vers l'avant (en moyenne 3 longueurs d'interaction hadronique), et à la valeur moyenne relativement basse (.5 GeV/c) de l'impulsion des hadrons (reconnus par interaction) comparée à celle des μ (1.5 GeV/c).

ii) Les ambiguïtés π/p restent après les critères de réjection de l'hypothèse p (présence de rayon δ , incompatibilité longueur-impulsion mesurée par courbure) sont aussi traitées par une méthode de pondération où la probabilité de chacune des hypothèses est déduite d'une comparaison du spectre des π^- et des traces ambiguës π/p . Cette pondération favorise à plus de 90 % l'hypothèse proton pour les traces d'impulsion supérieures à 1.GeV/c.

2. Les problèmes de l'estimation de l'énergie emportée par les neutres $\pi^o(\to \gamma\gamma)$ et neutrons, sont de deux origines :

1. ceux qui proviennent des γ et étoiles observées: des critères d' d'association sont déterminés à partir des événements sans ambiguïté d'association ;

2. ceux qui proviennent des neutres non détectés :

i) reconstruction du neutron lorsqu'une étoile a été associée à un vertex.
Ceci est accompli par une méthode cinématique où le neutron incident est reconstruit à partir de sa propore direction et de l'étoile observée ;

ii) perte des gammas non détectés. La valeur moyenne de l'énergie des gammas est ajoutée aux événements où un nombre impair de γ a été observé ;

iii) perte des neutrons non détectés: des spectres d'énergie des neutrons supposés identiques à ceux des protons, de la courbe d'inélasticité des interactions de neutrons et de la probabilité de matérialisation des neutrons dans la chambre, est déduite une énergie moyenne des neutrons non vus par intervalle d'énergie hadronique. Cette énergie est ajoutée aux événements, compte tenu de la multiplicité attendue en neutron.

3. Les effets des erreurs de mesure, des corrections pour neutres manquants et les effets nucléaires sont enfin évalués.
Outre l'incidence sur les valeurs mesurées, les effets nucléaires ont pour conséquence d'interdire la séparation expérimentale des candidats inélastiques et des candidats élastiques $\left(\nu_\mu\ n \to \mu^- p\ ,\ \bar{\nu}_\mu\ p \to \mu^+ n\right)$. Ceux-ci restent donc dans le lot analysé pour les sections efficaces différentielles.

4. Quelques coupures et soustractions sont appliquées sur le lot de candidats pour éliminer les bruits de fond (traces entrantes, interaction de neutrons ou de ν du type "courant neutre" : $\nu_\mu \left(\bar{\nu}_\mu\right) N \to \nu_\mu \left(\bar{\nu}_\mu\right) X$ événements provenant du flux défocalisé ν_μ en $\bar{\nu}$, $\bar{\nu}_\mu$ en ν) ou les événements mal mesurés $\left(E < 1\ \text{GeV}\ ,\ \frac{\Delta E}{E} > .3\right)$.

Les sections efficaces différentielles $\frac{d\sigma^{\nu,\bar{\nu}}}{dx}$, $\frac{d\sigma^{\nu,\bar{\nu}}}{dy}$ peuvent être alors déduites des distributions observées $\frac{dN^{\nu,\bar{\nu}}}{dx}$, $\frac{dN^{\nu,\bar{\nu}}}{dy}$.

Cette analyse fait l'objet de la troisième partie de ce travail. A cause de l'intérêt théorique de la comparaison à l'électroproduction, de la compatibilité des sections efficaces totales avec une croissance linéaire avec l'énergie, de la faible statistique et des erreurs expérimentales sur x et y qui interdisent de déterminer le détail du comportement des sections efficaces $\frac{d\sigma^{\nu,\bar{\nu}}}{dxdy}$, nous avons choisi d'analyser les sections efficaces différentielles dans l'optique d'une invariance d'échelle.

RESULTATS

Les distributions expérimentales sont trouvées compatibles compte tenu des erreurs expérimentales avec une dépendance des fonctions de structure (i) vis à vis de la seule variable x (au lieu de q^2 et ν) dans la région de haute énergie du plan (ν, q^2) accessible à notre expérience,

(ii) vis à vis de la variable $x' \equiv \frac{q^2}{2M\nu + M^2}$ dans toute la région ($E > 1$ GeV) analysée.

Les fonctions de structure, $F_i^{\nu,\bar{\nu}}(x)$, déterminées dans la région d'invariance d'échelle et $F_i^{\nu,\bar{\nu}}(x')$ déterminées dans tout le domaine d'énergie analysé, sont compatibles entre elles. Elles sont aussi compatibles avec la fonction de structure de l'électroproduction $F_2^{ed}(x)$.

Enfin les distributions en x et en y à toute énergie sont bien décrites par la superposition d'une contribution d'événements inélastiques (suivant la section efficace d'invariance d'échelle) et d'une contribution d'événements élastiques (suivant la section efficace élastique bien connue par d'autres expériences).

Faisant l'hypothèse que les fonctions de structure déterminées par les distributions en x' dans tout le domaine ($E > 1.$) sont identiques à $F_i^{\nu,\bar{\nu}}(x)$ dans la région d'invariance d'échelle, elles sont alors interprétées en termes de partons.

La confrontation des prédictions des différents modèles de partons aux mesures expérimentales est en faveur d'un modèle de partons de spin 1/2 (les spins entiers étant exclus); mais ne peut discriminer entre modèles à 3 ou 4 quarks de charge fractionnaire ou modèle de 3 triplets de quarks de charge entière (en-dessous du seuil de production de particules colorées).

Nous choisissons de nous placer dans le modèle à 3 quarks où les distributions de quarks, antiquarks, étranges ou non étranges peuvent être déterminées à partir des mesures de $\frac{d\sigma^{\nu,\bar{\nu}}}{dx'}$ et les fonctions de structure

de l'électroproduction. Ces distributions sont trouvées compatibles avec les modèles théoriques particuliers, mais les erreurs expérimentales sont grandes et de plus, les modèles diffèrent essentiellement à petit x où les données expérimentales sont très rares (et correspondent principalement à de petits q^2, donc loin de la région d'invariance d'échelle). De plus, l'interprétation en termes de partons des sections efficaces différentielles $\frac{d\sigma^{\nu,\bar{\nu}}}{dx'}$, dans tout le domaine $E > 1$ GeV, c'est-à-dire même à petit q^2 et ν, n'a pas de justification théorique solide.

Ces réserves faites, la compatibilité des résultats expérimentaux avec les modèles de quarks est remarquablement bonne, en particulier la comparaison des fonctions de structure de l'électroproduction et de ν-production.

Cette compatibilité ainsi que l'apparition précoce de l'invariance d'échelle des fonctions de structure $F_i^{\nu,\bar{\nu}}$: à 1. GeV si l'on choisit la variable x', dont l'interprétation théorique est encore ouverte, constituent les résultats essentiels de ce travail.

Digitized by the Internet Archive
in 2026

https://archive.org/details/IA41548106_0050

Submitted to
Nuclear Physics B

CERN/D.Ph.II/PHYS 74-32
21.08.74

EXPERIMENTAL STUDY OF STRUCTURE FUNCTIONS AND SUM RULES IN CHARGE-CHANGING INTERACTIONS OF NEUTRINOS AND ANTINEUTRINOS ON NUCLEONS

Gargamelle Neutrino Collaboration

H. Deden, F.J. Hasert, W. Krenz, J. von Krogh, D. Lanske, J. Morfin
K. Schultze and H. Weerts,
III. Physikalisches Institut der Technischen Hochschule, Aachen, Germany.

G.H. Bertrand-Coremans, J. Sacton, W. Van Doninck and P. Vilain*
Interuniversity Institute for High Energies, U.L.B., V.U.B., Brussels, Belgium.

D.C. Cundy, D. Haidt, M. Jaffre, S. Natali**, J.B.M. Pattison,
D.H. Perkins***, A. Rousset, W. Venus+ and H. Wachsmuth,
CERN, Geneva, Switzerland.

V. Brisson, B. Degrange, M. Haguenauer, L. Kluberg, U. Nguyen-Khac and
P. Petiau,
Laboratoire de Physique Nucleaire des Hautes Energies, Ecole Polytechnique,
Paris, France.

E. Bellotti, S. Bonetti, D. Cavalli, C. Conta++, E. Fiorini, C. Franzinetti+++,
A. Pullia and M. Rollier,
Istituto di Fisica dell'Universita, Milano and I.N.F.N. Milano, Italy

B. Aubert, L.M. Chounet, J. Gandsman, P. Heusse, L. Jauneau, C. Longuemare ,
A.M. Lutz, C. Pascaud and J.P. Vialle,
Laboratoire de l'Accelerateur Linéaire, Orsay, France.

F.W. Bullock, M.J. Esten, T.W. Jones, J. McKenzie, A.G. Michette[x], G. Myatt***
and W.G. Scott***[x],
University College, London, England.

---

* Chercheur agrée de l'Institut Inter-Universitaire des Sciences Nucléaires, Belgique.

** Now at the University of Bari.

*** Also at the University of Oxford.

\+ Now at the Rutherford High Energy Laboratory.

++ On leave of abscence from the University and INFN-Pavia.

+++ Also at the University of Turin.

x Supported by a Science Research Council grant

DDC/jr

ABSTRACT

The differential cross sections in freon (CF_3Br) of inclusive charge-changing neutrino and antineutrino interactions on nucleons, in the energy range E = 1 - 11 GeV, have been determined with respect to the Bjorken scaling variables $x = q^2/2M\nu$ and $y = \nu/E$. For $q^2 > 1$, $W^2 > 4$ GeV^2, the x and y distributions are consistent with scaling. In terms of the Bloom-Gilman variable $x' = q^2/(2M\nu + M^2)$, structure functions $\bar{F}_2^{\nu N}(x')$ and $\bar{F}_3^{\nu N}(x')$ can be defined and are found to be, within the errors of 10-20%, independent of E. $\bar{F}_2^{\nu N}(x')$ agrees well with the scaling function $3.6\ F_2^{eN}(x')$ for deep inelastic electroproduction on a nucleon. Assuming $\bar{F}_2$ and $\bar{F}_3$ represent the high energy asymptotic region, we find for the quark charge, the Gross/Llewellyn-Smith and the Adler sumrules:-

$$\int \bar{F}_2^{\nu N}\, dx' / \int F_2^{eN} dx' = 3.6 \pm 0.3 \qquad \text{(quark model: 3.6)}$$

$$\int \bar{F}_3^{\nu N}(x')dx' = 3.2 \pm 0.6 \qquad \text{(quark model: 2.9)}$$

$$(d\sigma^{\nu N} - d\sigma^{\bar{\nu}N})/dq^2 < 0.3\ G^2/\pi \qquad \text{for isoscalar target.}$$

The observed quark and antiquark momentum distributions are compatible with the predictions of quark-parton models fitted to electron scattering data.

1. INTRODUCTION

In a previous paper [1] results were presented on neutrino and antineutrino total cross sections measured with a focussed wideband beam at the CERN PS with the heavy-liquid bubble chamber Gargamelle (freon, CF_3Br, filling). It was observed that both $\sigma(\nu)$ and $\sigma(\bar{\nu})$ as well as the mean value of q^2, increased linearly with energy over the range E = 1 - 11 GeV, as would be expected from the Bjorken scaling hypothesis [2]. Furthermore, t ratio $\sigma(\bar{\nu})/\sigma(\nu)$ was found to have a mean value of 0.38 ± 0.02 and to be independent of energy.

In the present paper, we present results on the differential cross sections with respect to the scaling variables $y = \nu/E$ and $x = q^2/2M\nu$ or $x' = q^2/(2M\nu + M^2)$, where q^2 is the 4-momentum transfer squared and ν is the energy transfer from the neutrino to the nucleon in the rest-frame of the nucleon target. In the liquid employed, the neutron/proton ratio is 1.19, so that to a good approximation we can regard the cross sections as referring to isoscalar targets.

The data described here are based on analysis of a sample of 2656 neutrino and 1062 antineutrino interactions of energy greater than 1 GeV, observed among 87,730 and 166,680 pictures respectively. Details of the identification and measurement of events have been given in our previous paper, and we discuss here only those aspects which directly affect the determination and interpretation of the differential cross sections.

2. EXPERIMENTAL CONSIDERATIONS

2.1 Energy Resolution

Since the experiment is carried out in a wideband neutrino beam, the neutrino (antineutrino) energy in each event is taken as the sum of the energies of the visible secondaries, with suitable energy loss corrections.

The r.m.s. fractional errors in energy of the muon (E_μ) and in the energy (ν) transferred to secondary hadrons were estimated to be

$$(\Delta E_\mu / E_\mu) = 8\%$$
$$(\Delta \nu / \nu) = 15\% \qquad (1)$$

These errors are averaged over energy E and over all classes of event. There is little variation in the resolution with energy. As discussed in our previous paper, the hadron energy transfer has to be corrected for missing energy, of which undetected neutrons constitute the main cause. Based on events with observed neutron stars, and the detection efficiency (75%), an average neutron energy loss correction was applied to all events without neutrons. On average, secondary neutrons account for 4% of the energy in inelastic neutrino interactions and 8% in antineutrino. Thus, even large fluctuations in the neutron energy in individual events, about the average values obtained by the above procedure, have a small effect in comparison with other measurement errors, which are given in (1). However, for elastic events, expecially those produced by antineutrinos, $\bar{\nu} + p \rightarrow \mu^+ + n$, the estimated errors on ν are somewhat larger than for the inelastic events, and of order 20% on the basis of kinematic fitting.

2.2 Ambiguities

There are three sources of ambiguity which arise in the analysis of the events.

Firstly, neutrino/antineutrino ambiguities can arise when events contain both μ^+ and μ^- candidates. As discussed in our previous paper, these constitute a contamination of $< 2\%$ in the antineutrino events. The effects on the distributions are therefore negligibly small.

Secondly, self-ambiguous events, containing 2 muon candidates of the same sign (μ-π ambiguity) have to be taken into account. On average 10% of events are self-ambiguous. These can be treated (i) by weighting the unambiguous events, (ii) by taking all events and assigning (on the

basis of track length and energy), weight factors according to either hypothesis, to those which are ambiguous. The two methods give consistent results. The distributions given below are based on the second method.

A third source of ambiguity arises from uncertainty in the identification of positive charged hadron secondaries (π^+/p ambiguity), either because they interact after a short distance or because they are of high momentum (> 700 MeV/c). Approximately 20% of neutrino and 6% of antineutrino events contain such ambiguities. Using independent methods viz. the spectrum of interacting negative pions, the range spectrum of stopping protons, and by δ- ray analysis, it is inferred that most ($\gtrsim$ 75%) of the ambiguous secondaries are protons. None of the distributions given below is sensitive to the ambiguity assignment.

2.3 Fermi Motion

The structure functions which we are attempting to evaluate are functions of the invariant four-momentum transfer squared, q^2, and the energy transfer ν in the rest frame of the target nucleon, defined by $M\nu = P.q$ where P is the 4-momentum of the nucleon. When the energy transfer is measured in the laboratory frame, a smearing effect occurs because of Fermi motion in complex nuclei. We assume a distribution of Fermi momentum p of the form $\exp(-p^2/p_o^2).d^3p$, with $p_o = 0.2M$ as measured in electron-nucleus scattering experiments [20]. The error in ν arising from equating it to the laboratory hadronic energy transfer is almost symmetric [3] and of r.m.s. magnitude

$$\left(\frac{\Delta\nu}{\nu}\right)_{\text{Fermi}} = \pm\, 0.15\left(1 + \frac{q^2}{\nu^2}\right)^{\frac{1}{2}} \qquad (2)$$

The effects of Fermi motion on the experimental distributions are considered in detail below.

3. VERIFICATION OF BJORKEN SCALING

In the deep inelastic scaling region if the $\Delta S = 1$ contribution is neglected, the double differential cross sections have the form [2]

$$\underset{E\to\infty}{\text{Lt}} \quad \frac{d^2\sigma^{\nu N,\ \bar{\nu}N}}{dx\,dy} = \frac{G^2ME}{\pi} \left\{ (1 - y - y\frac{Mx}{2E})\ F_2(x) + \frac{y^2}{2}\,[2xF_1(x)] \pm y(1-\frac{y}{2})\,[xF_3(x)] \right\}$$

where $x = q^2/2M\nu$; $\quad 0 < x < 1$ (3)

$y = \nu/E$; $\quad 0 < y < (1 + \frac{Mx}{2E})^{-1}$

The cross sections as well as structure functions $F_{1,2,3}$ refer to averages over neutrons and protons(*). If we integrate over x and y, the ratio of total cross sections $R_1 = \sigma(\bar{\nu})/\sigma(\nu)$ determines limits on

$$A = \int 2xF_1(x)dx \Big/ \int F_2(x)dx$$

$$B = \int xF_3(x)dx \Big/ \int F_2(x)dx$$

In this experiment the ratio $R_1 = 0.38 \pm 0.02$, and if this ratio applies also in the scaling region, we obtain the previously quoted limits [1], $1 > A > 0.87$ and $0.90 > B > 0.85$. The first result is consistent with the Callan-Gross relation $2xF_1 = F_2$ for spin 1/2 constituents, which is strongly supported by the SLAC-MIT experiments [4]. We therefore assume $2xF_1 = F_2$ in what follows. If we integrate (3) the differential cross sections become

$$\frac{d\sigma}{dx}^{\nu N,\ \bar{\nu}N} = \frac{G^2ME}{3\pi}\,[2F_2^{\nu N}(x) \pm x\,F_3^{\nu N}(x)] \tag{4}$$

$$\frac{d\sigma}{dy}^{\nu N,\ \bar{\nu}N} = \frac{G^2ME}{\pi}\,[\int F_2^{\nu N}(x)dx][1-(1\mp B)(y-\frac{y^2}{2})] \tag{5}$$

---

*) F_3 is customarily defined with the opposite sign. That used here is for convenience only, with F_3 a positive quantity.

so that F_2 and F_3, and their integrals, can be separated using the x and y distributions. In these expressions, we have neglected terms in Mx/2E which contribute only at the per cent level for events in the scaling region.

The SLAC-MIT data show scaling for $q^2 > 1$ GeV^2, $W^2 > 4$ GeV^2. Within these cuts we have 200 neutrino events and 29 antineutrino events.

Fig. 1 shows the mean values, averaged over y, of $F_2(x)$ and $xF_3(x)$ in the scaling region $q^2 > 1$ GeV^2, $W^2 > 4$ GeV^2. The full-line curve in the F_2 plot is the quantity $3.6\ F_2^{eN}(x)$, where $F_2^{eN}(x)$ is an average over neutron and proton, taken from the electron-deuterium scattering data [4]. The factor 3.6 comes from the quark model and is discussed later. The dashed curve takes into account Fermi motion effects and measurement errors, as given in (1) and (2). There is agreement between the shape and magnitude of the SLAC curve and the present data. The agreement is independent of changes in the q^2 and W^2 cuts provided they remain inside the scaling region. Thus, within errors of order 10-20%, our data confirm scaling in inelastic neutrino interactions.

The curve in the plot of $xF_3(x)$ was computed from the quark and antiquark momentum distributions obtained by empirical fits to the electron-scattering data [14].

Fig. 2 shows the y distributions for events in the scaling region. The quantity plotted is

$$\frac{\pi}{G^2 M} \int \frac{1}{E} \frac{d^2\sigma}{dxdy}\, dx \Big/ \int 3.6\ F_2^{eN}(x)\, dx$$

where the range of integration is restricted by the scaling cuts to $0.1 < x < 0.6$. Within the large errors, the observed distributions are consistent with the formula (5) with B close to unity.

4. DIFFERENTIAL CROSS SECTIONS WITHOUT SCALING CUTS

In principle, data from inelastic neutrino scattering allow powerful tests of current algebra, and in particular of the sumrules derived from them. These predictions usually depend critically on the behaviour of the cross section at very small x values (typically of order 0.01) at large, fixed q^2 ($q^2 >> M^2$). It is obvious that such tests are not possible with any of the present generation of accelerators, yielding neutrino beams up to about 200 GeV energy only.

On the other hand, it is observed experimentally that some average type of scaling behaviour seems to hold down to low values of E and q^2; for example the constancy of $\sigma(\bar{\nu})/\sigma(\nu)$, and the linearity of $\sigma(\nu)$, $\sigma(\bar{\nu})$ and $\langle q^2 \rangle$ with energy, are observed down to $E \sim 1$ GeV. This has prompted us to investigate distributions without any scaling cuts, in the low energy, low q^2 region. While the distribution we obtain in the parameter y shows departures from scaling behaviour, those in the parameter $x' = q^2/(2M\nu + M^2)$ of Bloom and Gilman [5] are not only independent of cuts in y or E, as remarked previously [6], but in striking agreement with the SLAC data in the scaling region. We therefore felt it important to analyse the x' distributions in detail.

4.1 The x' distributions

Our reasons for choosing the Bloom-Gilman parameter x' in preference to the Bjorken variable x are as follows:

(i) In the SLAC-MIT data, it is observed that the approach to scaling, as W^2 is increased from low values, occurs faster in x' than in x.

(ii) The relation between $\langle q^2 \rangle$ and E can be fitted [1] by a straight line which does not however pass through the origin, exactly as predicted if x' is the relevant variable in the low energy region [6].

(iii) At low energies, a considerable fraction of the total cross sectio is contributed by elastic events. These can occur only at $x = 1$ while all other exclusive channels have $x < 1$. On the other hand, the parameter $x' = q^2/(q^2 + W^2)$, so that elastic events ($W = M$) are treated on the same footing as other resonances, and can populate the region $0 < x' < 1$. In principle, it should of course be possible to remove elastic events from the sample and consider inelastics only. This is undesirable in that the scaling concept is intended to apply to a complete set of final hadron states, and in practice difficult because there are experimental problems in discriminating cleanly between elastic and inelastic events.

(iv) The distorting effects of Fermi smearing and measurement errors are particularly severe for elastic events, when they are plotted as a function of the Bjorken variable x. The effects of errors on the distributions in x' are however greatly reduced, for both elastic and inelastic events.

In presenting the distributions in x', we have arbitrarily defined functions $\bar{F}_2(x')$ and $\bar{F}_3(x')$ which are obtained from equation (4) simply by replacing x everywhere by x'. Fig. 3 gives values of $\bar{F}_2(x',E)$ for various energy ranges. The agreement, within errors of 10-20%, between the shape and magnitude of $\bar{F}_2(x'E)$ and the SLAC data, for all E values, suggests that x' is a relevant scaling variable to employ in the low-energy region.

A point to note is that the elastic events themselves yield a distribution in x' which is of similar shape to the scaling curve at low energy ($E < 2$ GeV) although somewhat broader at higher energy. Such behaviour is generally expected on the basis of the fall-off with q^2 of the elastic fo factors, for $x' > 0.1$, and because of the Pauli principle in complex nuclei, which inhibits the elastic cross-section at small x'.

In the following analysis we assume that the distributions in x' observed at low energies do in fact correspond to the x distributions in the scaling region. This is an empirical assumption which is consistent with the data available.

4.2 PCAC and CVC predictions at small x'

Fig. 4 shows all data ($1 < E < 11$ GeV) on $\bar{F}_2(x')$ together with the SLAC scaling curve. Fig. 5 gives $x'\bar{F}_3(x')$, together with predictions based on empirical fits of quark-parton models to the electron data. $x'\bar{F}_3(x')$ is closely equal to $\bar{F}_2(x')$ for $x' > 0.3$, but significantly less for smaller x'.

At finite energy, when $q^2 \to 0$ as $x' \to 0$, the behaviour of $x'\bar{F}_3(x')$ and $\bar{F}_2(x')$ can be argued on the basis of the CVC and PCAC hypotheses. The former ensures that the V-A interference term $x'\bar{F}_3(x')$ must vanish, while PCAC relates $\bar{F}_2(x')$ to the pion-nucleon cross section. If it is permissible to interchange the scaling limit ($q^2 > 1$, $E \to \infty$) by ($q^2 \to 0$, E finite) then [9,15] PCAC predicts $\bar{F}_2(0) \sim 0.3$ if one allows a factor 2 reduction for nuclear shadowing.

In the asymptotic scaling region, $q^2 > 1$, $x \to 0$, $\nu \to \infty$, a similar behaviour is expected on the basis of Regge exchange in the t-channel for the appropriate forward elastic scattering amplitude, and Pomeron dominance as $x \to 0$. The prediction is that $F_2(0) \to$ constant, and that the interference term $xF_3(x)$ should vanish. The Regge limit on $F_2(0) \sim 0.2$-0.4 on the basis of empirical fits to the electron scattering data [13,14,15,17].

The results in Figs. 4 and 5 are consistent with the above predictions $\bar{F}_2(x') \to$ constant and $x'F_3(x') \to 0$ as $x' \to 0$, even though our events are far from the asymptotic region. The PCAC prediction is expected to be valid in the first bin, $x' = 0 - 0.01$, where $q^2 \sim m_\pi^2$.

4.3 The y-Distributions

The distributions in y, without scaling cuts, are given in Figs. 6 and 7 for various energy ranges.

As expected, the antineutrino cross sections fall off more rapidly with y than do those for neutrinos. The main features can be understood on a qualitative basis. First we note from (5) that in the limit of infinitely high energy and for B = 0.85, scaling predicts an approximately flat neutrino distribution, and one for antineutrinos varying roughly as $(1-y)^2$. At finite energy, however, we expect a sharp peak at small y values due to the elastic channel, which is dominated by form factors falling off very rapidly with q^2 (= 2MEy in elastic events). The situation is quite different from that for the x' distribution, where elastic events are spread broadly over the range x' = 0 → 1.

In addition to the peak near y = 0, the kinematically allowed range in x' is from 0 to $x'_{max} = 4E^2(1-y)/(M^2+2MyE)$, so that at finite energy there should also be a sharp fall-off of the distributions close to y = 1. The data in Figs. 6 and 7 exhibit these general qualitative features. By way of illustration we have calculated the y distribution by combining two contributions : one corresponding to the elastic events according to the known elastic form factors, the other to the inelastic events for which we have assumed the same differential cross section $d^2\sigma/dx'dy$ as in the scaling region (Figs 1 and 2); the effects due to Fermi motion and experimental errors have been taken into account.

5. COMPARISON OF EXPERIMENTAL DATA WITH THE QUARK MODEL

5.1 Quark Charges

The neutrino and electron scattering data have in common that they require spin 1/2 for the elementary point like constituents (partons) in terms of which scale invariance may be interpreted. It is therefore natural to discuss a model of a nucleon built from quarks and quark-antiquark pairs [2]. Assuming isospin 1/2 quarks with the fractional charge assignment

of Gell-Mann and Zweig, we have for the $\Delta S = 0$ part of the weak cross section [19],

$$\int F_2^{\nu N} dx / \int F_2^{eN} dx \leq \frac{18}{5} = 3.6 \qquad (7)$$

where $F_2^{eN} = 1/2\ (F_2^{ep} + F_2^{en}) = 1/2\ F_2^{ed}$, and the inequality becomes an equality if the contribution of strange quarks and antiquarks to the electron cross section can be neglected. This appears reasonable, since from the ratio $\sigma(\bar{\nu})/\sigma(\nu) = 0.38$, it is known that non-strange antiquarks make only $\sim$ 5% contribution.

From our previous analysis [1] it was found that , using the ratio and difference of neutrino and antineutrino cross sections, and assuming that these apply to the scaling region,

$$0.49 \pm 0.03 \leq \int F_2^{\nu N} dx \leq 0.51 \pm 0.03 \qquad (8)$$

Minor corrections need to be applied to this estimate, to take account of the small $\Delta S = 1$ part of the cross section, and for the n/p ratio in freon ($S = 1.19$), to obtain $F_2(\Delta S = 0)$ on an isoscalar target ($n = p$). These two corrections increase the integral by 3.5%, giving [7]

$$\left[\int F_2^{\nu N} dx\right]_{\substack{\Delta S=0 \\ n=p}} = 0.52 \pm 0.03 \qquad (9)$$

to be compared with the electroproduction data [4]:-

$$\int (F_2^{ep} + F_2^{en})\, dx = 0.29 \pm 0.02$$

The ratio

$$\left[\int F_2^{\nu N} dx\right]_{\Delta S = 0} / \int F_2^{eN} dx = 3.59 \pm 0.31 \qquad (10)$$

supports the quark model (7), albeit with large errors. This result

tests the fractional charge assignments for quarks(*). In common with the electron data, the result (9) requires 50% of the nucleon momentum to be carried by inactive constituents (gluons). Deviations from (7) due, for example, to new quantum numbers like "charm" are generally expected to be small [16],typically an order of magnitude smaller than the error in the result (10).

5.2 The Number of "Valence" Quarks; The Gross/Llewellyn-Smith Sumrule

For a nucleon target of baryon number and hypercharge B = Y = 1, composed of Gell-Mann/Zweig quarks, the sumrule [8] has the form for either neutron or proton targets,

$$\begin{aligned} 1/2\int(F_3^{\nu} + F_3^{\bar{\nu}})dx &= 2B + Y + (I_3 - 3Y/2)\sin^2\Theta \\ 1/2\int(F_3^{\nu p} + F_3^{\nu n})dx &= 3/2\ (1 + \cos^2\Theta) \end{aligned} \qquad (11)$$

where Θ is the Cabbibo angle and we have assumed SU3 symmetry. For the SU4 model of Glashow, Iliopoulos and Maiani [21], the integral has the value 3 exactly. The sumrule corresponds to the number of "valence" quarks in a nucleon, with zero strangeness and charm, $(N-\bar{N}) = 3$, and is a direct test of the fractional baryon number assignment of 1/3 for the quarks.

In attempting to test (11) experimentally, account has to be taken of the fact that, in the medium employed, the neutron/proton ratio S is not unity (S = 1.19 in freon). This means that, in using equation (4) to define $F_3^{\nu N}$, we obtain

$$\begin{aligned} \left[\int F_3^{\nu N}dx\right]_{\text{freon}} = &\int\left[\frac{\left(F_3^{\nu p} + F_3^{\bar{\nu}p}\right) + S\left(F_3^{\nu n} + F_3^{\bar{\nu}n}\right)}{2(S+1)}\right]dx \\ &+ \int\left[\frac{\left(F_2^{\nu p} - F_2^{\bar{\nu}p}\right) + S\left(F_2^{\nu n} - F_2^{\bar{\nu}n}\right)}{(S+1)}\right]dx/x, \end{aligned} \qquad (12)$$

---

*) It should be noted[7] that the $\Delta I = 1$ rule, $|V| = |A|$ coupling of the currents and 10% isoscalar contribution in electroproduction also predict a ratio 4 x 0.9 = 3.6

where the second term is very small and may be evaluated assuming the Adler sumrule. Thus, with $\cos^2\theta = 0.95$ we find

$$\left[\int F_3^{\nu N} dx\right]_{freon} = \frac{3\cos^2\theta(2S+1) - (S+2)}{(S+1)} = 2.94 \text{ (SU3)} \qquad (12a)$$

$$= \frac{(5S+1)}{(S+1)} = 3.17 \text{ (SU4)} \qquad (12b)$$

From the data in Fig. 5, we can estimate the integral (12), assuming that, in the low energy region, we may replace x by x' as hypothesized above. It is also necessary, in order to evaluate the integral down to x' = 0, to assume that $\bar{F}_3(x')$ is well behaved at the origin (otherwise, the GLS integral could be divergent).

The result of our analysis is that

$$\int_0^1 \bar{F}_3(x')dx' = 3.2 \pm 0.6 \qquad E > 1 \text{ GeV}$$

$$= 3.0 \pm 0.6 \qquad E > 2 \text{ GeV} \qquad (13)$$

where the error includes both statistical and flux errors. In addition, some distortion of the $\bar{F}_3(x')$ distribution will occur on account of errors in measurement of x'. For example, at very small values of x', of order 0.003, uncertainties in the muon angle, relative to the neutrino, can become important. The effect of such measurement errors depends on the exact form of the $\bar{F}_3(x')$ distribution near the origin. As an example, if one assumes the form for $\bar{F}_3(x')$ suggested by empirical fits of quark/antiquark momentum distributions to the electron scattering data, the systematic effect of errors on the Gross-Llewellyn Smith integral is of order 5% only, and can therefore be neglected in comparison with the statistical error.

The result (13) supports the quark model (12). Fig. 8 shows the integral (13) plotted as a function of energy. At each energy, the integral has been evaluated using the measured differential cross sections

for neutrinos and antineutrinos. The rate of convergence of the sumrule is of interest. Our data indicate 50% saturation if the lower limit of the integral is x' = 0.08, and 80% saturation for x' = 0.02.

5.3 The Quark and Antiquark Momentum Distributions

From the values of $\bar{F}_2$ and $\bar{F}_3$ derived above, and assuming they represent the scaling limit, we obtain the quark momentum distributions. Calling $N(x')dx'$ and $\bar{N}(x')dx'$ the number of quarks/antiquarks with fractional nucleon momentum x', and $Q(x')$, $\bar{Q}(x')$ the total momentum carried by quarks/antiquarks in unit interval at x', then

$$\bar{Q}(x') = x'\bar{N}(x') = [\bar{F}_2(x') - x'\bar{F}_3(x')]/2$$
$$Q(x') = x'N(x') = [\bar{F}_2(x') + x'\bar{F}_3(x')]/2 \qquad (14)$$

The distributions are given in fig. 9. Assuming $x'\bar{F}_3(x') \to 0$ as $x' \to 0$, we expect $Q(0) = \bar{Q}(0)$, as observed. Whereas $\bar{Q}(x')$ drops off with increasing x', $Q(x')$ rises sharply to a maximum at $x' \sim 0.1$. For $x' > 0.4$, $\bar{Q}$ is slightly negative. This may be due to small errors of a few percent in the overall $\bar{\nu}/\nu$ cross section ratio, used in normalizing the distributions. In their general form, these results are in fair agreement with the predictions of various models (see for example, Landshoff and Polkinghorne [13], Mc Elhaney and Tuan [14], Altarelli et al [17]).

6. THE ADLER SUMRULE AND CHARGE SYMMETRY

In some models of hadrons extra quantum numbers, in addition to isospin and strangeness, are introduced (see de Rujula and Glashow [10] for a list). These may modify the Adler sumrule [11], causing deviations from charge symmetry, and can therefore be investigated even with I = 0 targets.

The so-called β - sumrule of Adler is a fixed q^2, infinite energy sumrule which is independent of scaling. For a target of isospin component

I_3 and hypercharge Y, it has the form:-

$$\underset{E\to\infty}{\text{Lt}} \left(\frac{d\sigma^{\nu}}{dq^2} - \frac{d\sigma^{\bar{\nu}}}{dq^2}\right) = \frac{-G^2}{2\pi} \left[4I_3\cos^2\theta + (2I_3 + 3Y)\sin^2\theta\right] \qquad (15)$$

assuming SU3. As before, the SU4 version is obtained by setting $\theta = 0$. For a medium with neutron/proton ratio S, this becomes, if we denote by $\sigma^{\nu N}$, $\sigma^{\bar{\nu}N}$ the cross sections per nucleon of the target

$$\underset{E\to\infty}{\text{Lt}} \left(\frac{d\sigma^{\nu N} - d\sigma^{\bar{\nu}N}}{dq^2}\right) = \frac{G^2}{\pi} \frac{[(S-1)\cos^2\theta - (S+2)\sin^2\theta]}{(S+1)} \qquad (16)$$

$$= 0.008\ G^2/\pi \qquad \text{(SU3)}$$

$$\underset{E\to\infty}{\text{Lt}} \left(\frac{d\sigma^{\nu N} - d\sigma^{\bar{\nu}N}}{dq^2}\right) = \frac{G^2}{\pi} \frac{(S-1)}{(S+1)}$$

$$= 0.087\ G^2/\pi \qquad \text{(SU4)}$$

There are two interesting aspects of the Adler sumrule. The first relates to its rate of convergence, the second to deviations due to possible breakdown of charge symmetry.

6.1 Convergence for isoscalar targets

In order to investigate (16) in our low-energy region, we plot in Fig. 10 our data on $(d\sigma^{\nu N} - d\sigma^{\bar{\nu}N})/dq^2$ in freon, as a function of the quantity $V_o = q^2/2ME$. Clearly errors are too large to verify the sumrule itself, but are consistent with it.

The rate of saturation of the Adler sumrule has been frequently discussed [12] in the context of scaling i.e., in the limit $q^2 > 1$, $E \to \infty$, $x \to 0$, where it takes the form:-

$$\underset{\substack{E\to\infty \\ q^2 \text{ finite}}}{\text{Lt}} \frac{(d\sigma^{\nu p} - d\sigma^{\bar{\nu}p})}{dq^2} = \underset{x_o\to 0}{\text{Lt}} \frac{G^2}{2\pi} \int_{x_o}^{1} \frac{(F_2^{\nu p} - F_2^{\bar{\nu}p})}{x}$$

For a target consisting of a mixture of protons and neutrons, the corresponding integral can be computed in terms of the lower limit, x_o, or equivalently $V_o = q^2/2ME$, if the forms of both $F_2(x)$ and $F_3(x)$ are known on both protons and neutrons [18]. For an isoscalar target, it turns out however that the integral, for finite x_o or V_o, depends almost exclusively on $F_3(x)$ averaged over neutrons and protons. The full curve in Fig. 10 was computed using an empirical expression for $F_3(x)$ using quark momentum distributions derived from a fit to electron scattering data [14]. The curve is in satisfactory agreement with the neutrino data, which, it must be emphasized once more, are mostly outside the scaling region. The empirical model used for $F_3(x)$ also predicts 90% saturation of the Adler sumrule on hydrogen by $x_o \sim 0.005$ ($\omega_o \sim 200$).

6.2 Deviations from the Adler Sumrule

A reasonable extrapolation of the data in Fig. 10 to $V_o \to 0$ sets an upper limit to possible deviations from the sumrule. Thus

$$\lim_{V_o \to 0} \left\{ \left(\frac{d\sigma - d\bar{\sigma}}{dq^2}\right)_{\text{observed}} - \left(\frac{d\sigma - d\bar{\sigma}}{dq^2}\right)_{\text{Adler}} \right\} < 0.3 \frac{G^2}{\pi} \qquad (17)$$

For convenience the results (10), (13) and (17) are summarized in the Table, together with the asymptotic predictions of the charmless Gell-Mann/Zweig quark model and three models with charm. The present experiment is at low energy and presumably below threshold for exciting new quantum numbers. No deviations from the Gell-Mann/Zweig model are observed. These results show that precise, high energy experiments with a few thousand events should be able not only to detect charm, if it exists, but differentiate clearly between the various charm models.

Table of Sumrules, per nucleon in freon

Quantity	Observed value	SU3 (fractional charge)	SU4 Quartet charm	Triplet charm (Beg & Zee [22])	Triplet charm (Achiman [23])
$F_2^{\nu N}dx / F_2^{eN}dx$	3.6 ± 0.3	∿ 3.6	∿ 3.6		
$\bar{F}_3^{\nu N}dx'$ (see equ.(12))	3.2 ± 0.6	2.94	3.17	-16.4	+ 5.2
$\frac{\pi}{G^2} \frac{d\sigma^{\nu N} - d\sigma^{\nu N}}{dq^2}$ $(q^2/E \to 0$	< 0.3	0.008	0.087	-8.2	-4.1

7. CONCLUSIONS

The results of the foregoing analysis may be summarised as follows:-

i) For $q^2 > 1$, $W^2 > 4$ the distributions in $x = q^2/2M\nu$ and $y = \nu/E$ are consistent with scaling.

ii) The cross sections with respect to $x' = q^2/(2M\nu + M^2)$ can be used to define functions $\bar{F}_2(x')$ and $\bar{F}_3(x')$ which appear to be independent of energy E. Further, the quantity $\bar{F}_2(x')$ agrees in shape with

$F_2^{eN}(x')$ deduced from electron scattering experiments. The ratio $\int F_2^{\nu N} dx' / \int F_2^{eN} dx' = 3.6 \pm 0.3$, in agreement with the fractional charge quark model.

iii) By identifying the quantities $\bar{F}_2(x')$ and $\bar{F}_3(x')$ with $F_2(x)$ and $F_3(x)$ in the scaling region, we have investigated the experimental validity of asymptotic sumrules. Our data are in good agreement with the Gross/Llewellyn-Smith sumrule for the triplet quark model, with quarks of baryon number 1/3. We find no detectable deviations from the Adler sumrule.

iv) The distributions in $\bar{F}_2(x')$ and $\bar{F}_3(x')$ and the quark (antiquark) momentum distributions are in excellent agreement with models fitted empirically to the electron scattering data.

v) The data described here are taken at low energy, where the conditions considered necessary for application of the naive parton model do not apply. Thus, perhaps the most significant result of this analysis is that the asymptotic predictions appear to be borne out, within errors of order 10%, even in the low energy region.

REFERENCES

[1] Eichten T. et al., Phys.Lett. 46B (1973) 274.

[2] Bjorken J.D., Phys.Rev. 179 (1969) 1547,
Bjorken J.D. and Paschos, E.A., Phys.Rev. 185 (1969) 1975,
Phys.Rev. D1 (1970) 3151.

[3] There is a slight skewing in the $\Delta\nu$ distribution to higher values, arising from the dependence of the cross section on the centre of mass energy and hence on the direction of the Fermi momentum p. This leads to an average 2% overestimate of ν for E = 1.5 GeV, falling to 1.5% at E = 10 GeV. This effect is neglected.

[4] Bodek A. et al., Phys.Rev.Lett. 30 (1973) 1087,
Bodek A., MIT thesis (1973),
Miller G. et al., Phys.Rev. D5 (1972) 528.

[5] Bloom E. and Gilman F., Phys.Rev.Lett. 25 (1970) 1140.

[6] Myatt G. and Perkins D.H., Phys.Lett. 34B (1971) 542.

[7] Perkins D.H., Proc. XVI Int.Conf. H.E. Physics, Batavia;
4 (1972) 216.

[8] Gross D.J. and Llewellyn-Smith C.H., Nucl.Phys. B14 (1969)337.

[9] Budny, R.V., Phys.Rev. D2 (1970) 1271.

[10] de Rujula A. and Glashow S. (Harvard preprint 1973).

[11] Adler S.L., Phys.Rev. 143 (1966) 1144.

[12] Bjorken J.D., and Tuan S.F., Comments Nucl.Part.Phys. 5 (1972) 71.

[13] Landshoff P. and Polkinghorne J., Phys.Lett. 34B (1971) 621.

[14] McElhaney R. and Tuan S.F., Phys.Rev. D8 (1973) 2267,
See also J.T. Dakin and G.J. Feldman, Phys.Rev. D8 (1973) 2862.

[15] Suzuki M., Nucl.Phys. B66 (1973) 368.

[16] Novoseller D. and Ravndal F., CALT 68 (1974) 440.

[17] Altarelli G., Cabibbo N., Maiani L. and Petronzio R., CERN Th. 1757 (1974).

[18] From equation (3) it can be shown that, for a lower limit $v_o = q^2/2ME \neq 0$, (16) will be replaced by

$$\left(\frac{d\sigma^{\nu N} - d\sigma^{\bar{\nu}N}}{dq^2}\right) = \frac{G^2}{\pi}\left\{\int_{v_o}^{1} \left(\frac{F_2^{\nu N} - F_2^{\bar{\nu}N}}{2x}\right)\left(1-(v_o/x) + (v_o^2/2x^2)\right)dx\right.$$

$$\left. + \int_{v_o}^{1} \left(\frac{F_3^{\nu N} + F_3^{\bar{\nu}N}}{2}\right)\left((v_o/x)-(v_o^2/2x^2)\right)dx\right\}$$

The first integral is clearly smaller than the Adler limit (16) for $v_o = 0$, and the main contribution comes from the second term.

In Fig. 10, the integral above has been computed using the quark momentum distributions of McElhaney and Tuan [14] from a fit to electron scattering data:-

$$xF_3(x) = 1.74x^{1/2}(1 - x)^3(1 + 2.3x) + 1.11x^{1/2}(1 - x)^{3.1}$$

[19] If one includes $\Delta S = 1$ processes, and inserts the value for the Cabbibo angle, the limit 18/5 is modified to 69/20 = 3.45. [16]

[20] D. Zeller, PhD Thesis, Karlsruhe (1973),
G. Campos Venuti et al., ISS/72/9 Roma (1972).

[21] Glashow S.L., J. Iliopoulos and L. Maiani, Phys.Rev. D2 (1973) 675.

[22] Bég M.A. and A. Zee, Phys.Rev.Lett. 30 (1973) 675.

[23] Achiman Y., Nucl.Phys. B56 (1973) 635.

FIGURE CAPTIONS

Fig. 1 (a) The scaling function $F_2^{\nu N}(x)$ computed from the neutrino and antineutrino differential cross sections, for the cut $q^2 > 1$ GeV^2, $W^2 > 4$ GeV^2, where W = final state hadron mass. The solid curve $3.6\ F_2^{eN}(x)$ is a fit to the SLAC electron-nucleon scattering data, where the factor 3.6 comes from the quark model. The dashed curve indicates the modification due to Fermi smearing and measurement errors.

(b) The interference term $xF_3^{\nu N}(x)$ computed from the data in the scaling region. The curve is that calculated using quark/anti-quark distribution functions obtained from empirical fits [14] to electron scattering data.

Fig. 2 Distributions in $y = \nu/E$ for neutrino and antineutrino events, in the scaling region. In each case the quantity plotted is

$$(\pi/G^2M)\int \frac{1}{E}\ \frac{d^2\sigma}{dxdy}\ dx \Big/ \int 3.6F_2^{eN}(x)dx,$$

where the range of integration is restricted by the scaling cuts to the interval $0.1 < x < 0.6$. The curves were calculated from equation (3) assuming $2xF_1(x) = F_2(x)$ and $xF_3(x) = 0.9F_2(x)$ in the range $0.1 < x < 0.6$. At the energies accessible in this experiment, data exist for the scaling region only in the interval $0.3 < y < 1.0$.

Fig. 3 $\bar{F}_2^{\nu N}(x',E)$ deduced from equation (4) by replacing $x = q^2/2M\nu$ by the Bloom-Gilman variable $x' = q^2/(2M\nu + M^2)$, and without any cuts in q^2 or W^2. In each energy range, the SLAC curve of $3.6F_2^{eN}(x')$ is given, together with the modification expected from Fermi smearing and measurement errors.

Fig. 4 $\bar{F}_2^{\nu N}(x')$ computed from all events irrespective of neutrino/antineutrino energy. At small x', the data are binned in small intervals $\Delta x'$ to indicate the fall in $\bar{F}_2$. Within the statistical errors the form of $\bar{F}_2$ for $x' < 0.1$ is independent of energy.

Fig. 5 Values of $x'\bar{F}_3^{\nu N}(x')$ computed for all events, without cuts in q^2 or W^2. The curves show typical predictions, based on empirical fits of quark momentum distributions to electron scattering data.

Fig. 6 Neutrino events: y distributions by bins of neutrino energy. The empty circles correspond to elastic events, the full circles to all events. The solid lines are expected distributions computed from the elastic form factors, and from the structure functions in the scaling region.

Fig. 7 The y distributions for antineutrino events. The curves shown are calculated as in Fig. 6.

Fig. 8 The integral $\int\bar{F}_3(x')dx'$ evaluated as a function of energy. The horizontal broken line shows the value, $\int F_3^{\nu N}(x)dx = 2.94$ predicted at asymptotically high energy from the Gross Llewellyn Smith sumrule [8].

Fig. 9 The quantities $x'\bar{N}(x') = [\bar{F}_2(x') - x'\bar{F}_3(x')]/2$ and $x'N(x') = [\bar{F}_2(x') + x'\bar{F}_3(x')]/2$ deduced from the distributions in Figs. 4 and 5. At asymptotically high energies, these would represent the distributions of total momentum carried by the antiquarks and quarks respectively. The areas under the two distributions represent the fractional nucleon momentum carried by all antiquark or quark constituents. The curves represent the asymptotic predictions of Landshoff and Polkinghorne [13], McElhaney and Tuan [14] and Altarelli et al [17], in all cases based on fits of quark momentum distributions to electron scattering data.

Fig. 10 The data on $(d\sigma^{\nu N} - d\sigma^{\bar{\nu}})/dq^2$ in freon, plotted against $v_o = q^2/2ME$. The curve shows the scaling prediction for $v_o > 0$, using an empirical fit to F_3 from electron scattering data, [14].

STRUCTURE FUNCTIONS FOR EVENTS IN THE SCALING REGION $q^2 > 1$ GeV^2 $W^2 > 4$ GeV^2

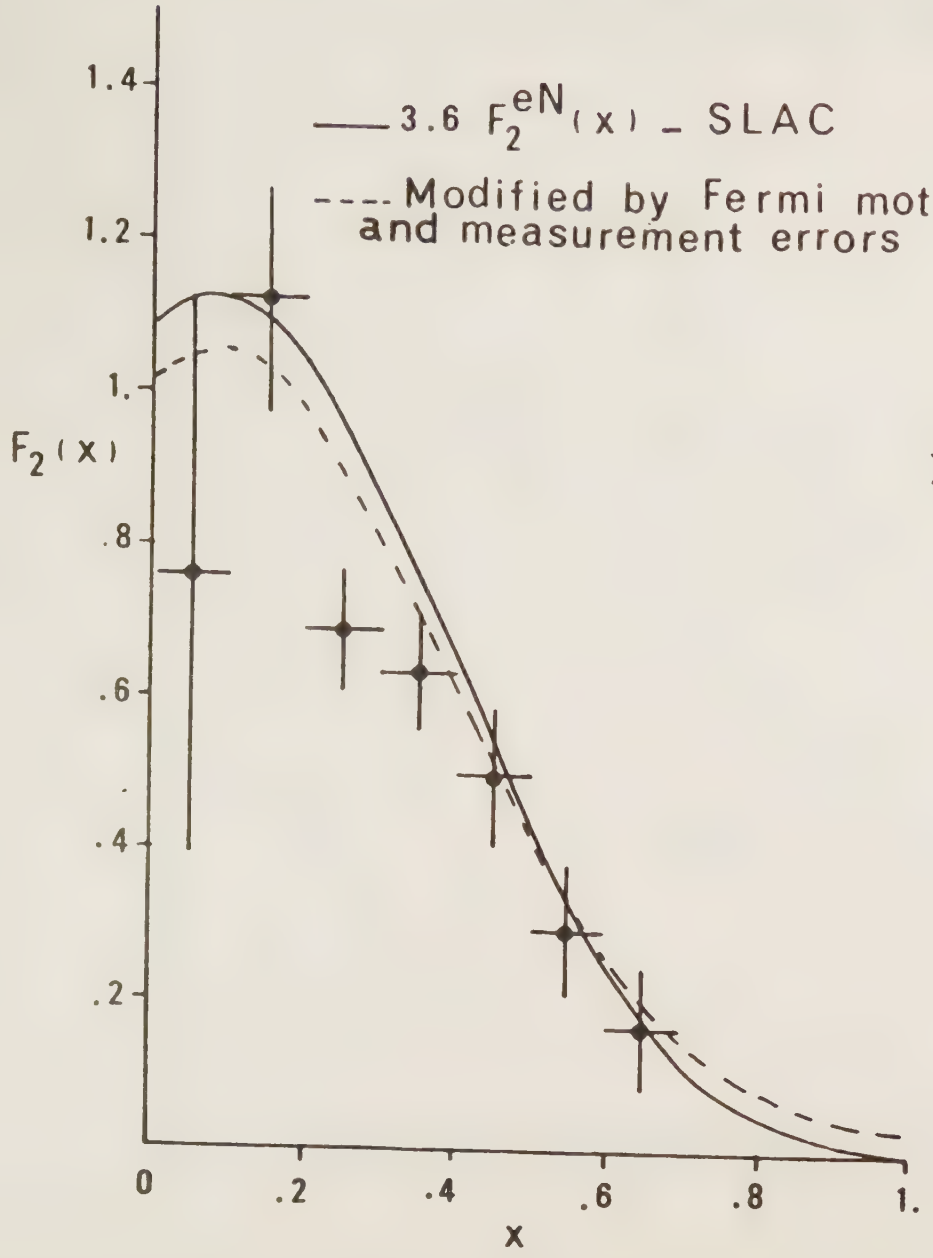

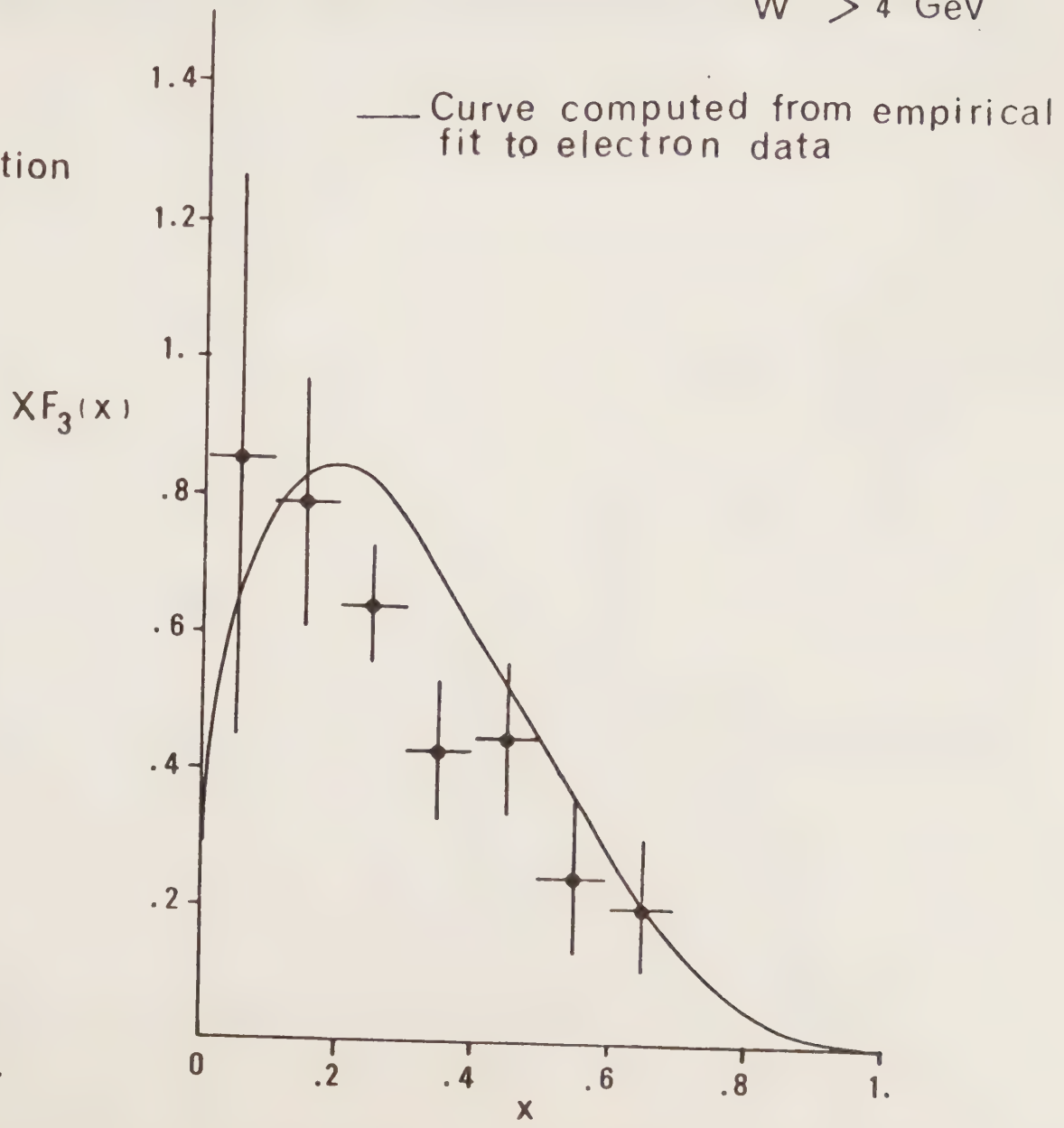

FIG. 2

y-DISTRIBUTIONS FOR EVENTS IN THE SCALING REGION $q^2 > 1\,GeV^2$, $W^2 > 4\,GeV^2$

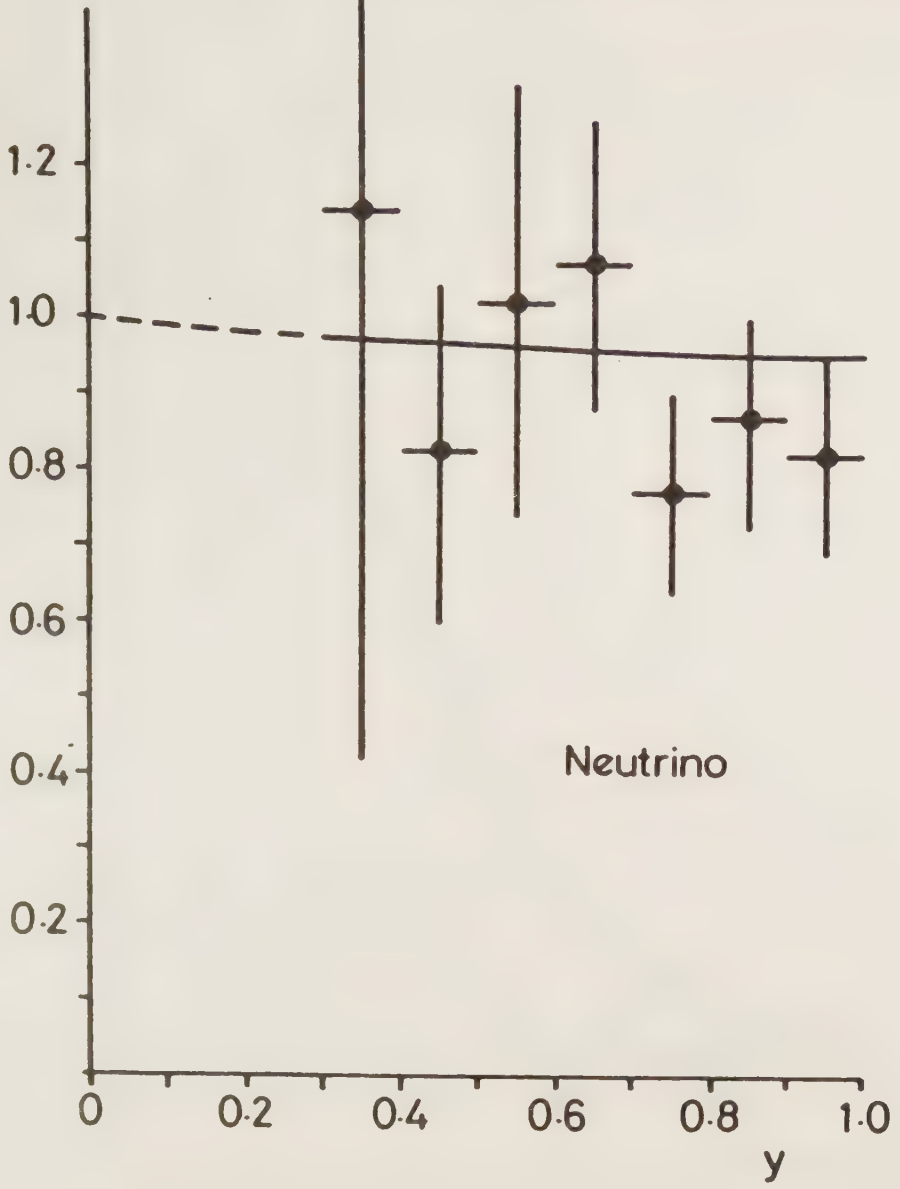

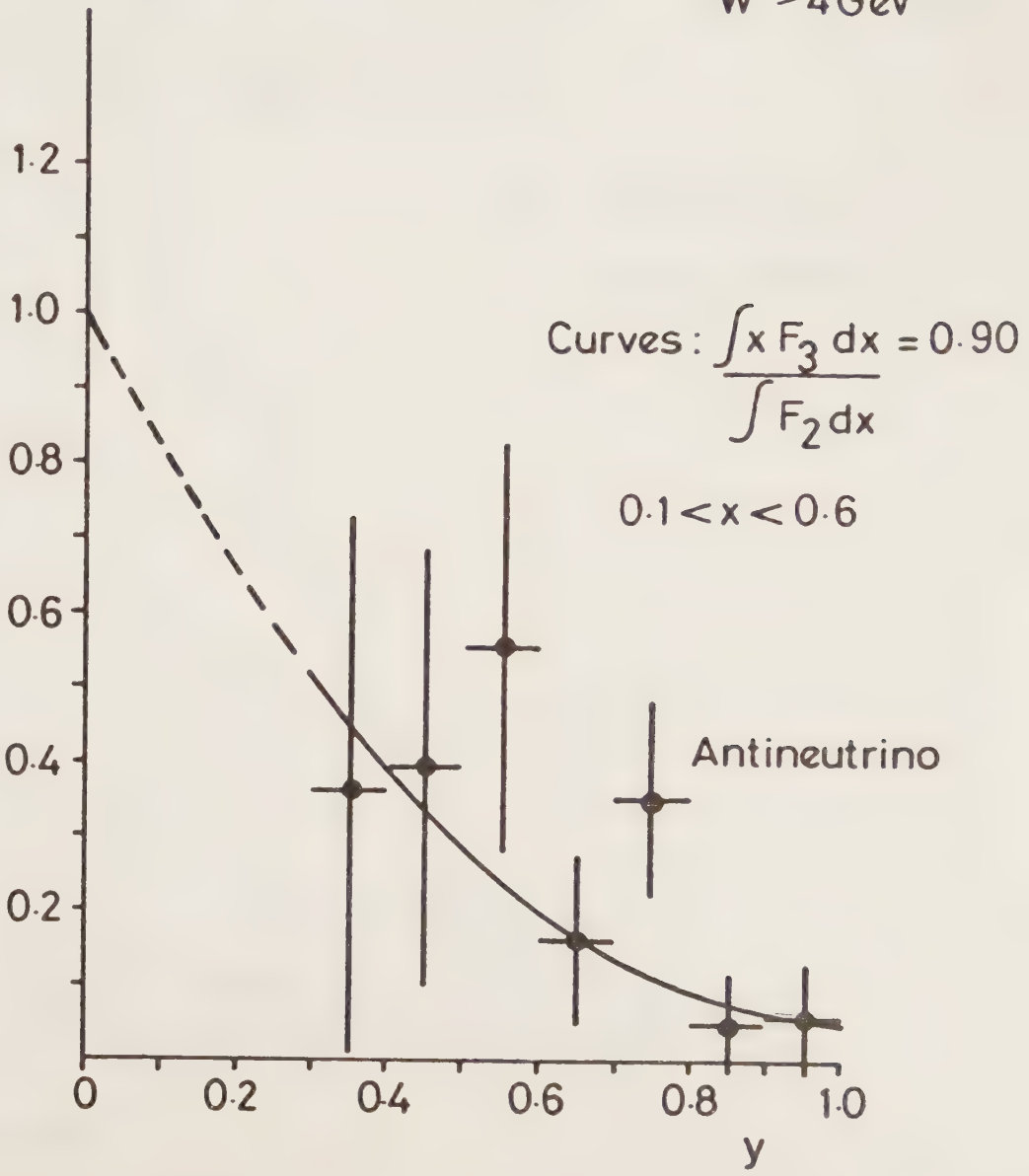

FIG.3

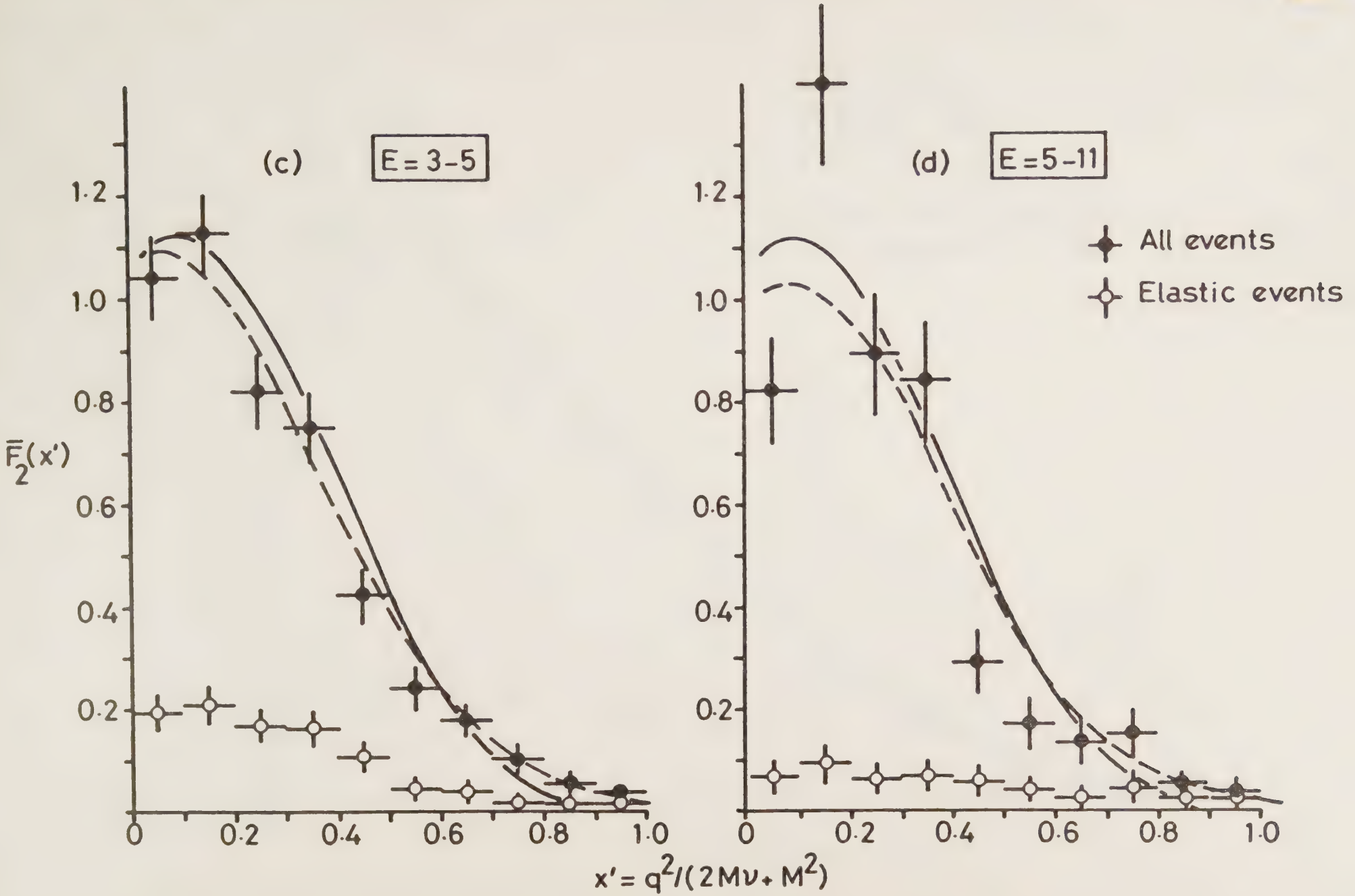
(c)
E = 3-5
(d)
E = 5-11
All events
Elastic events
$\bar{F}_2(x')$
1·2
1·0
0·8
0·6
0·4
0·2
0
0·2
0·4
0·6
0·8
1·0
$x' = q^2/(2M\nu + M^2)$

FIG. 4

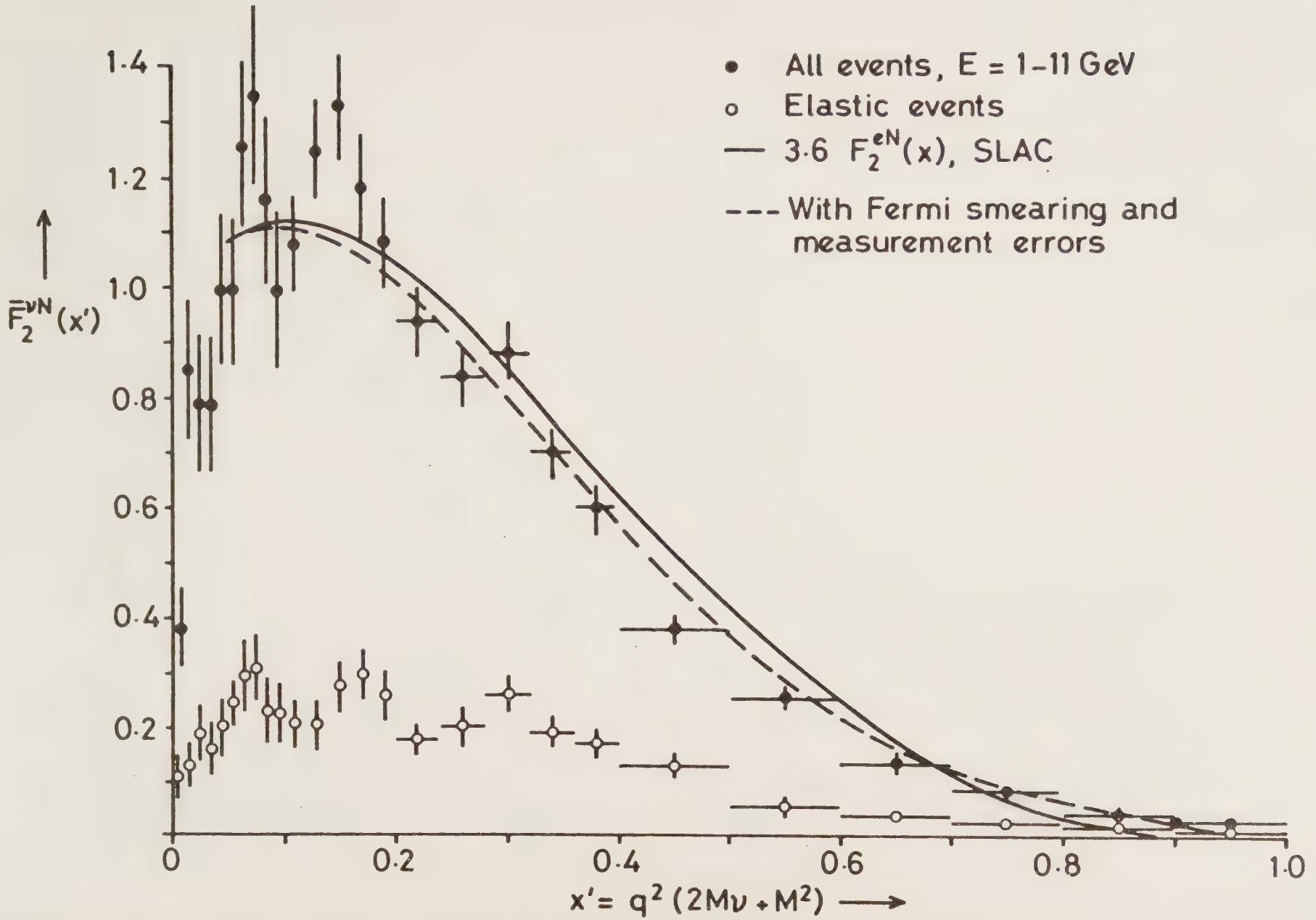
All events, E = 1–11 GeV
Elastic events
3·6 $F_2^{eN}(x)$, SLAC
With Fermi smearing and measurement errors
$\bar{F}_2^{\nu N}(x')$
1·4
1·2
1·0
0·8
0·6
0·4
0·2
0
0·2
0·4
0·6
0·8
1·0
$x' = q^2/(2M\nu + M^2)$

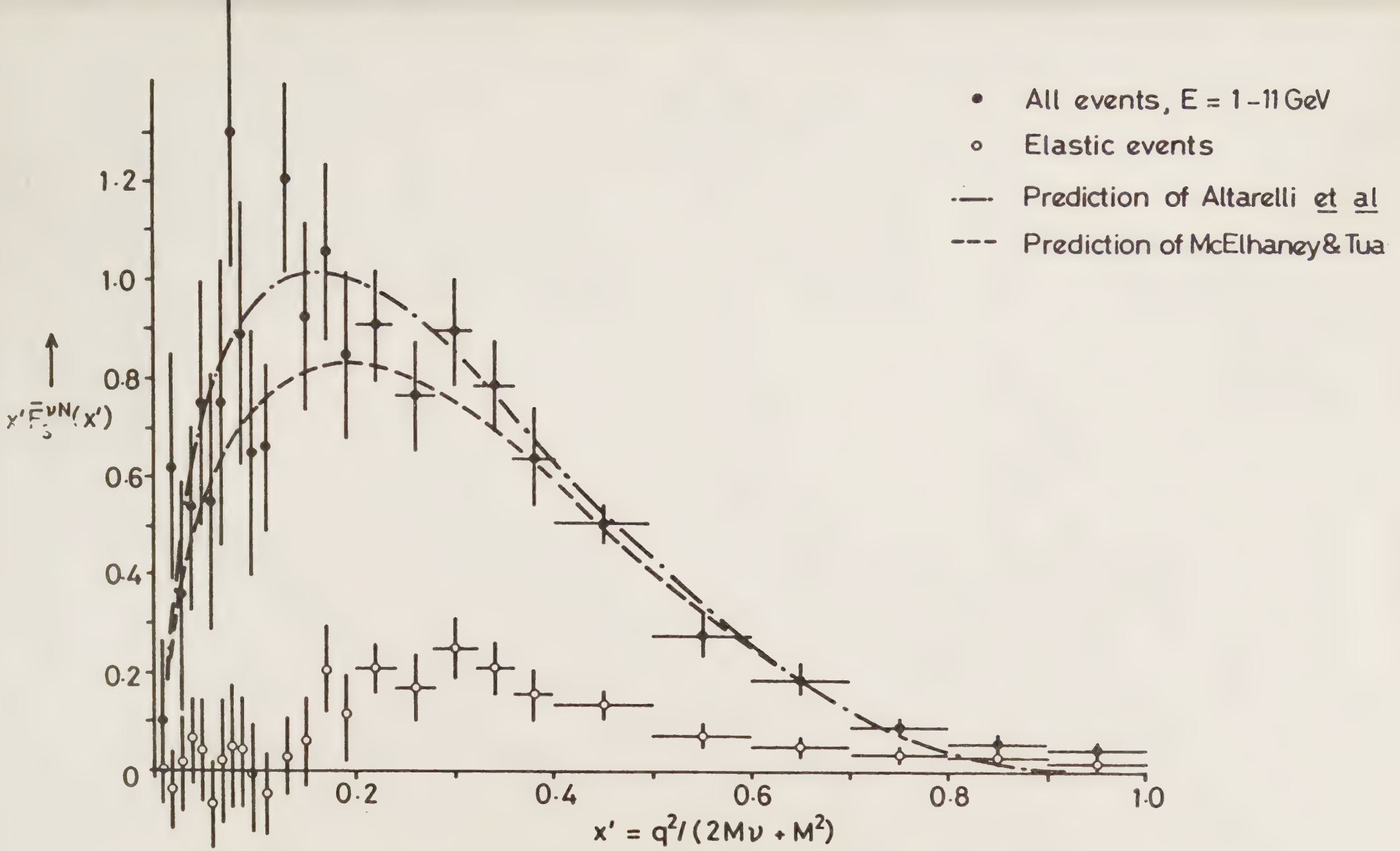
All events, E = 1–11 GeV
Elastic events
Prediction of Altarelli et al
Prediction of McElhaney & Tuan
$x'\bar{F}_3^{\nu N}(x')$
1·2
1·0
0·8
0·6
0·4
0·2
0
0·2
0·4
0·6
0·8
1·0
$x' = q^2/(2M\nu + M^2)$

Fig 6

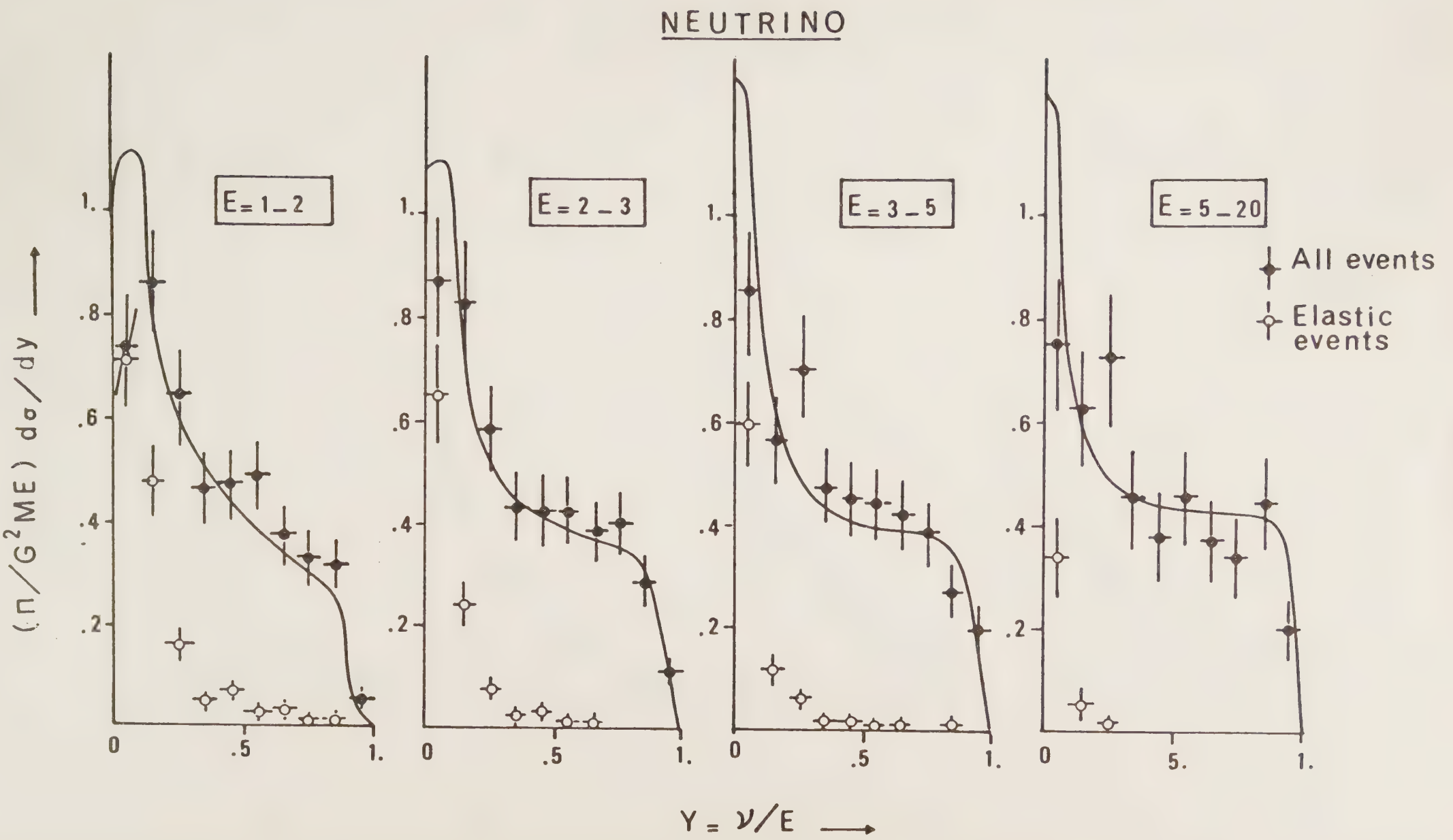
NEUTRINO
E = 1 _ 2
E = 2 _ 3
E = 3 _ 5
E = 5 _ 20
All events
Elastic events
(n/G²ME) dσ/dy
Y = ν/E
0
.5
1.
5.
.2
.4
.6
.8

Fig 7

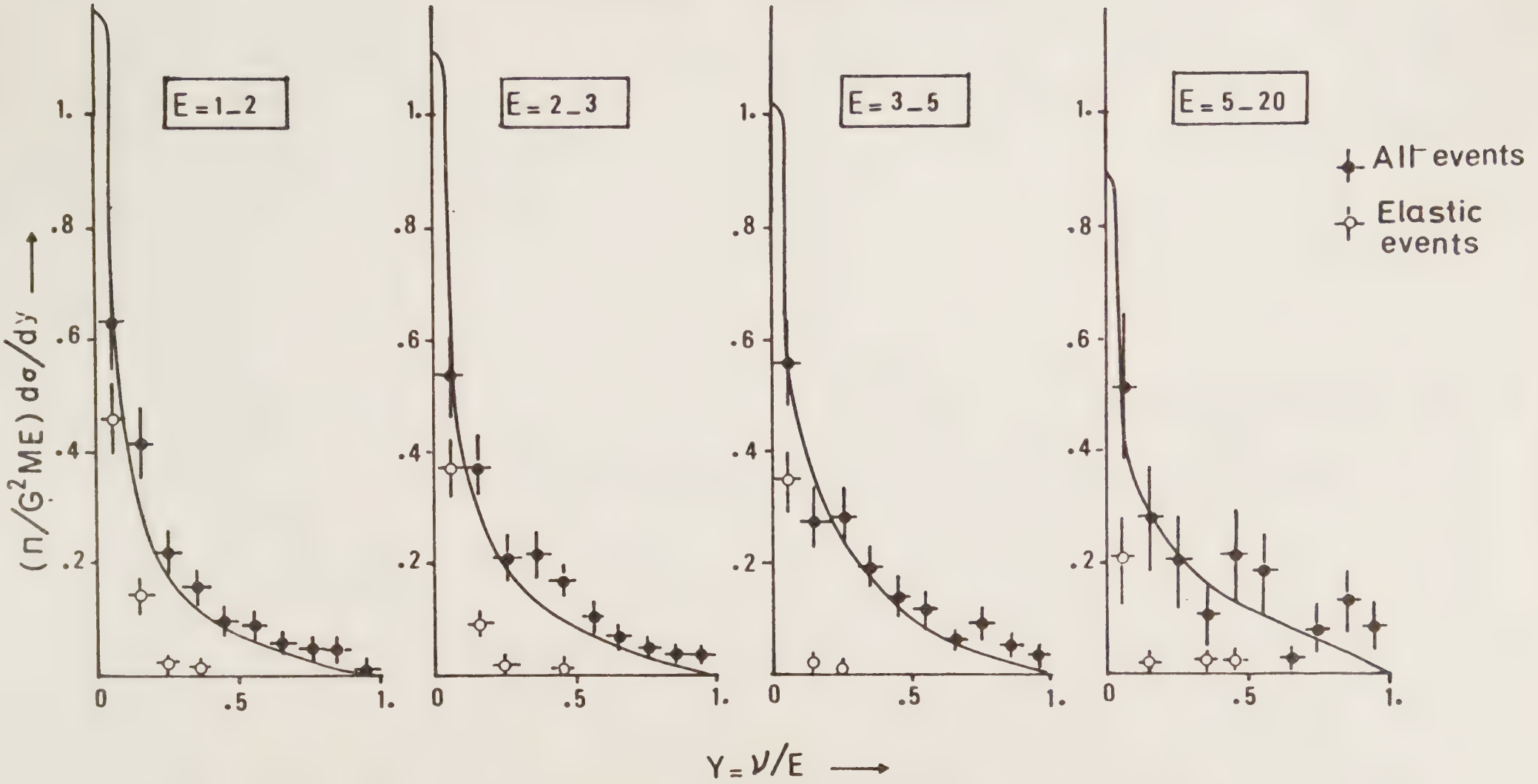
ANTINEUTRINO
E = 1_2
E = 2_3
E = 3_5
E = 5_20
All events
Elastic events
(n/G²ME) dσ/dy
Y = ν/E
0
.2
.4
.6
.8
1.
.5

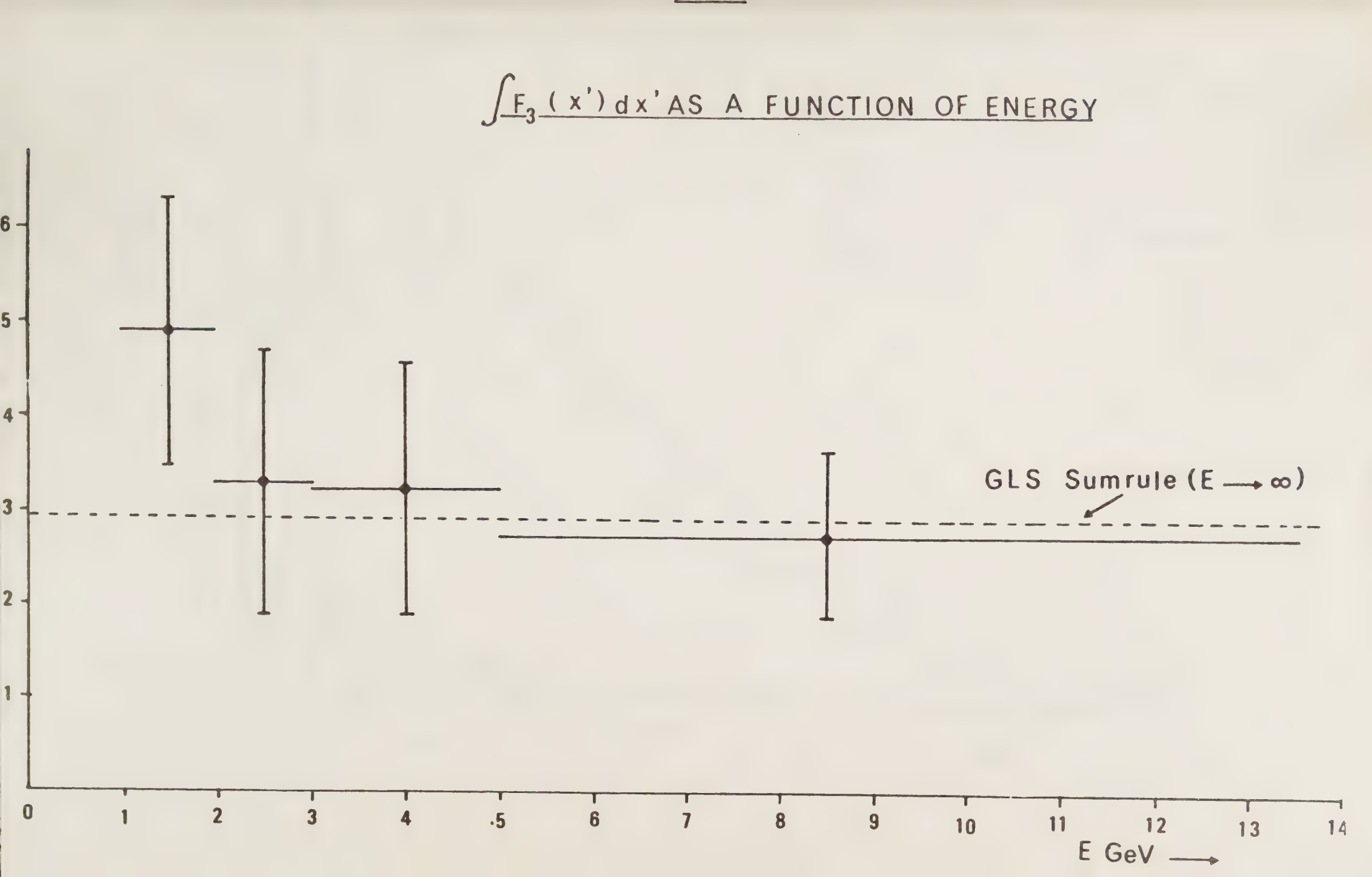
$\int F_3(x')dx'$ AS A FUNCTION OF ENERGY
6
5
4
3
2
1
GLS Sumrule (E ⟶ ∞)
0
1
2
3
4
.5
6
7
8
9
10
11
12
13
14
E GeV ⟶

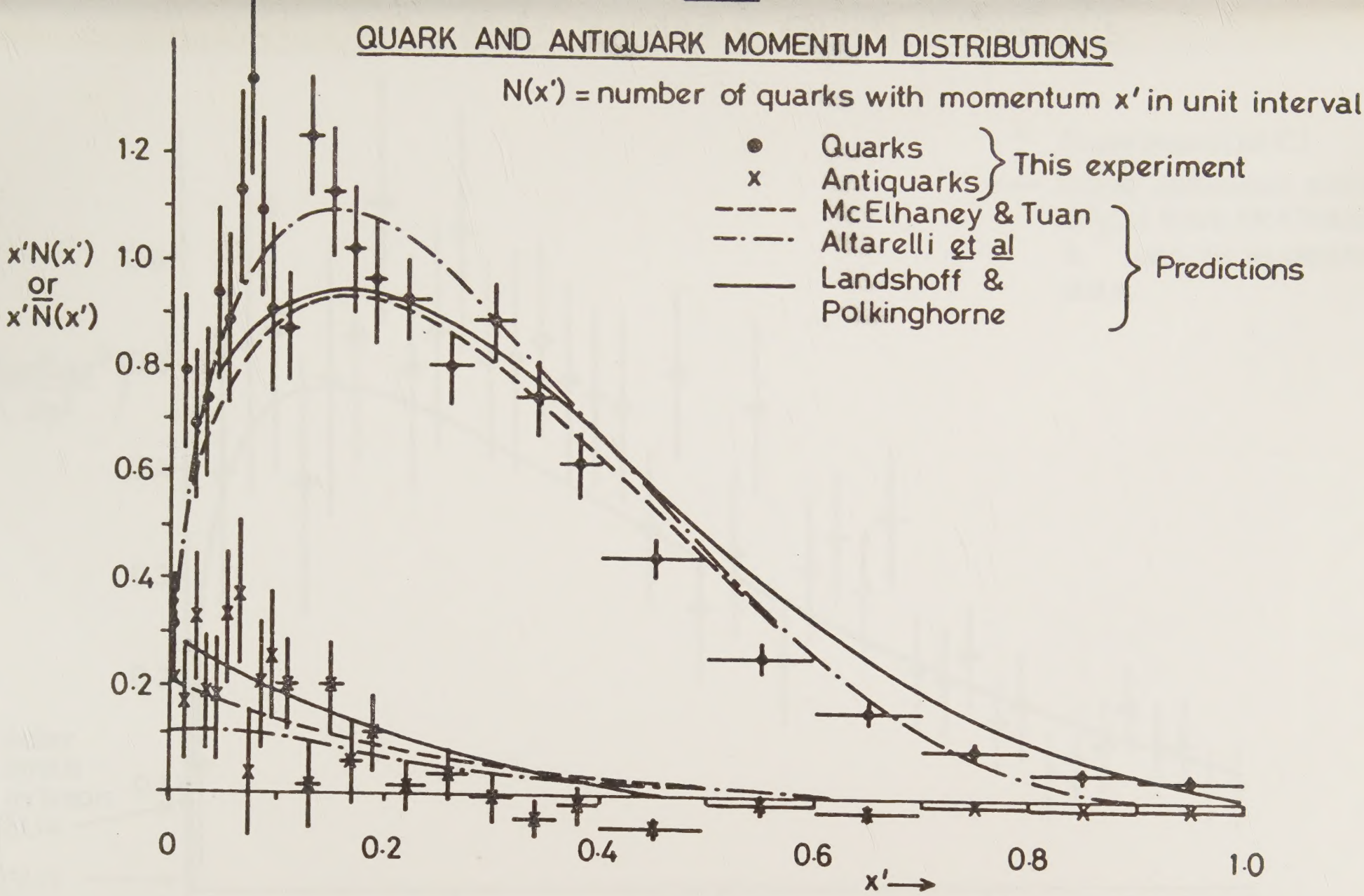
QUARK AND ANTIQUARK MOMENTUM DISTRIBUTIONS
N(x') = number of quarks with momentum x' in unit interval
Quarks
Antiquarks
This experiment
McElhaney & Tuan
Altarelli et al
Landshoff & Polkinghorne
Predictions
x'N(x') or x'N̄(x')
1·2
1·0
0·8
0·6
0·4
0·2
0
0·2
0·4
0·6
0·8
1·0
x'

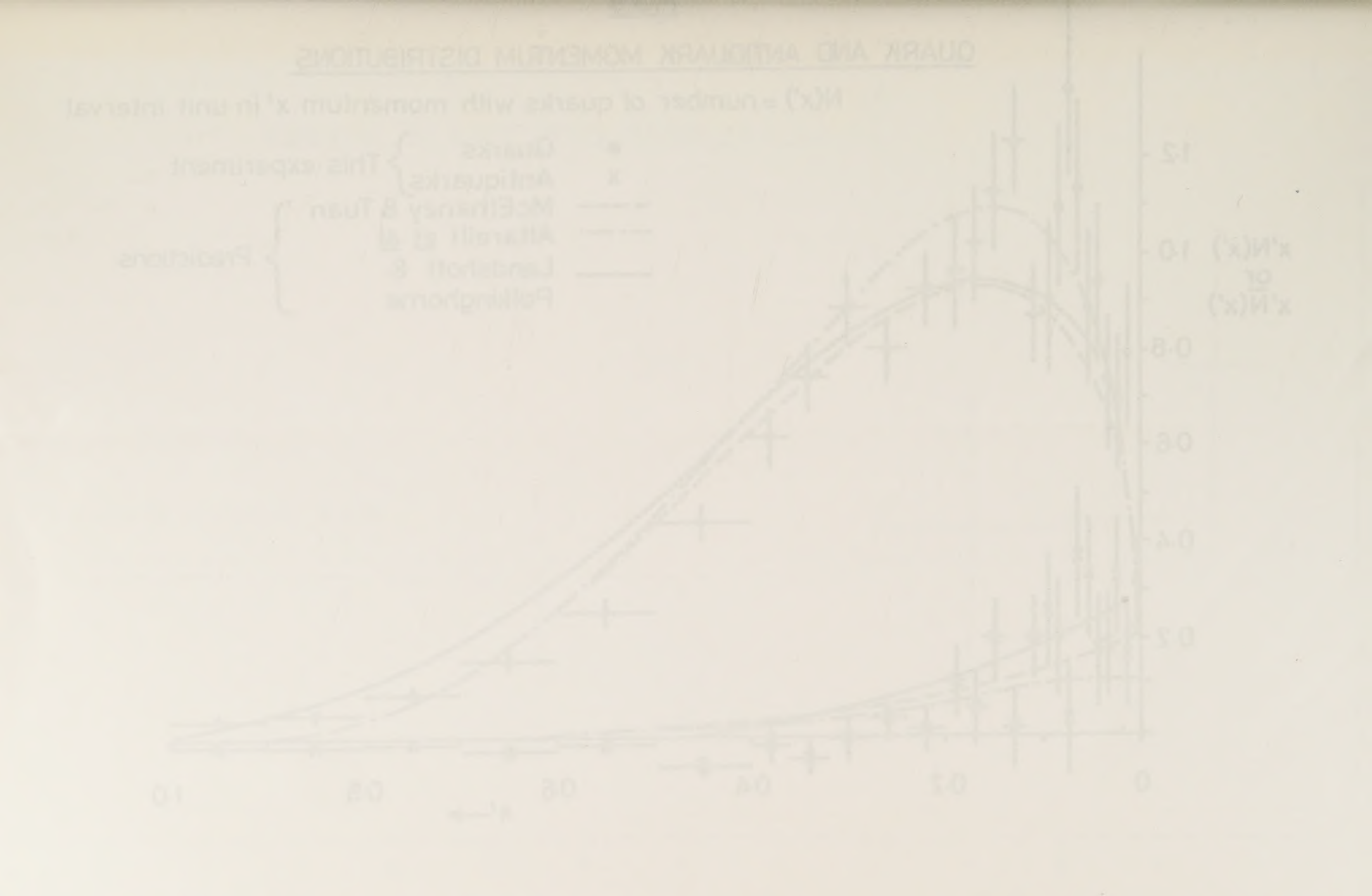
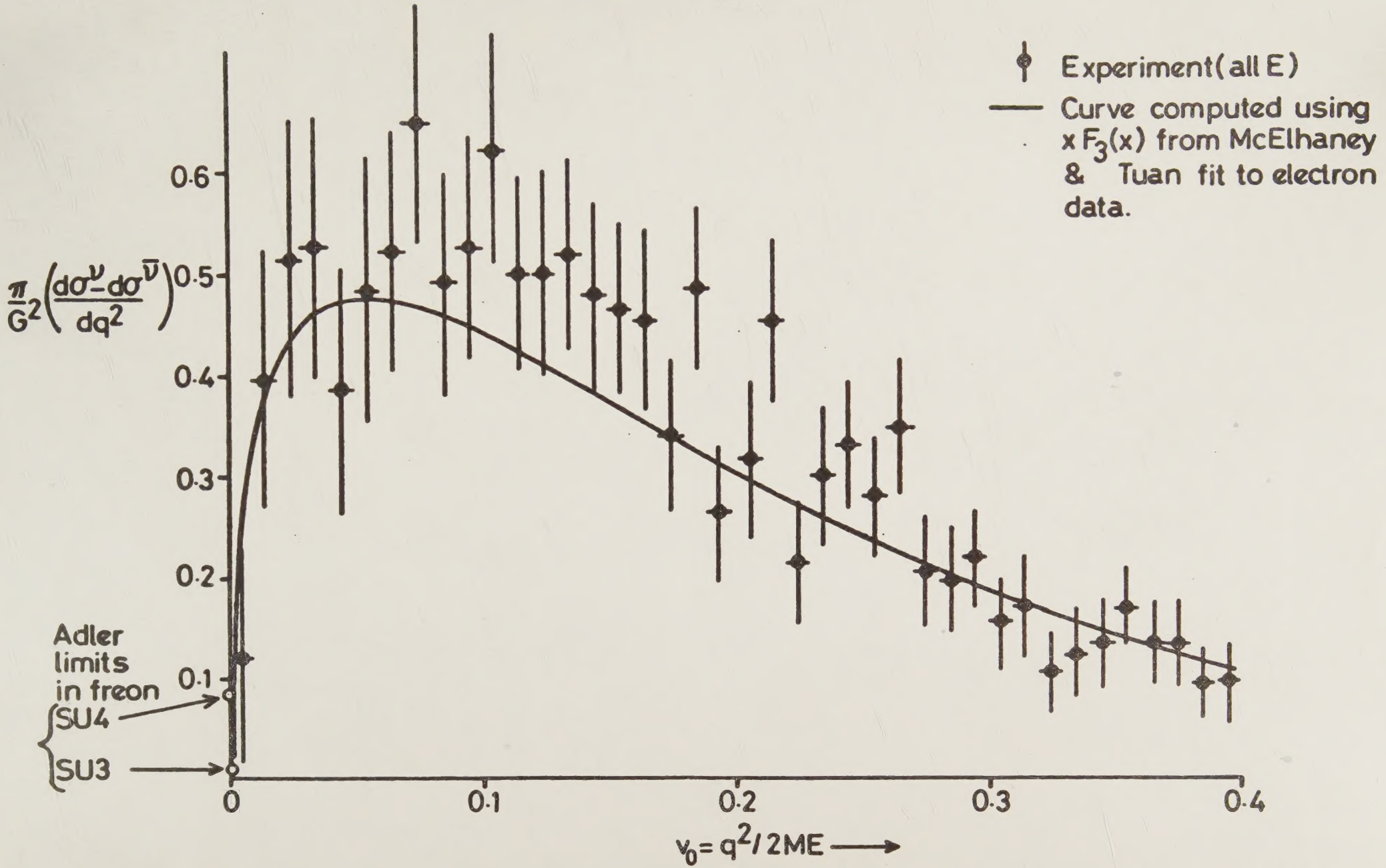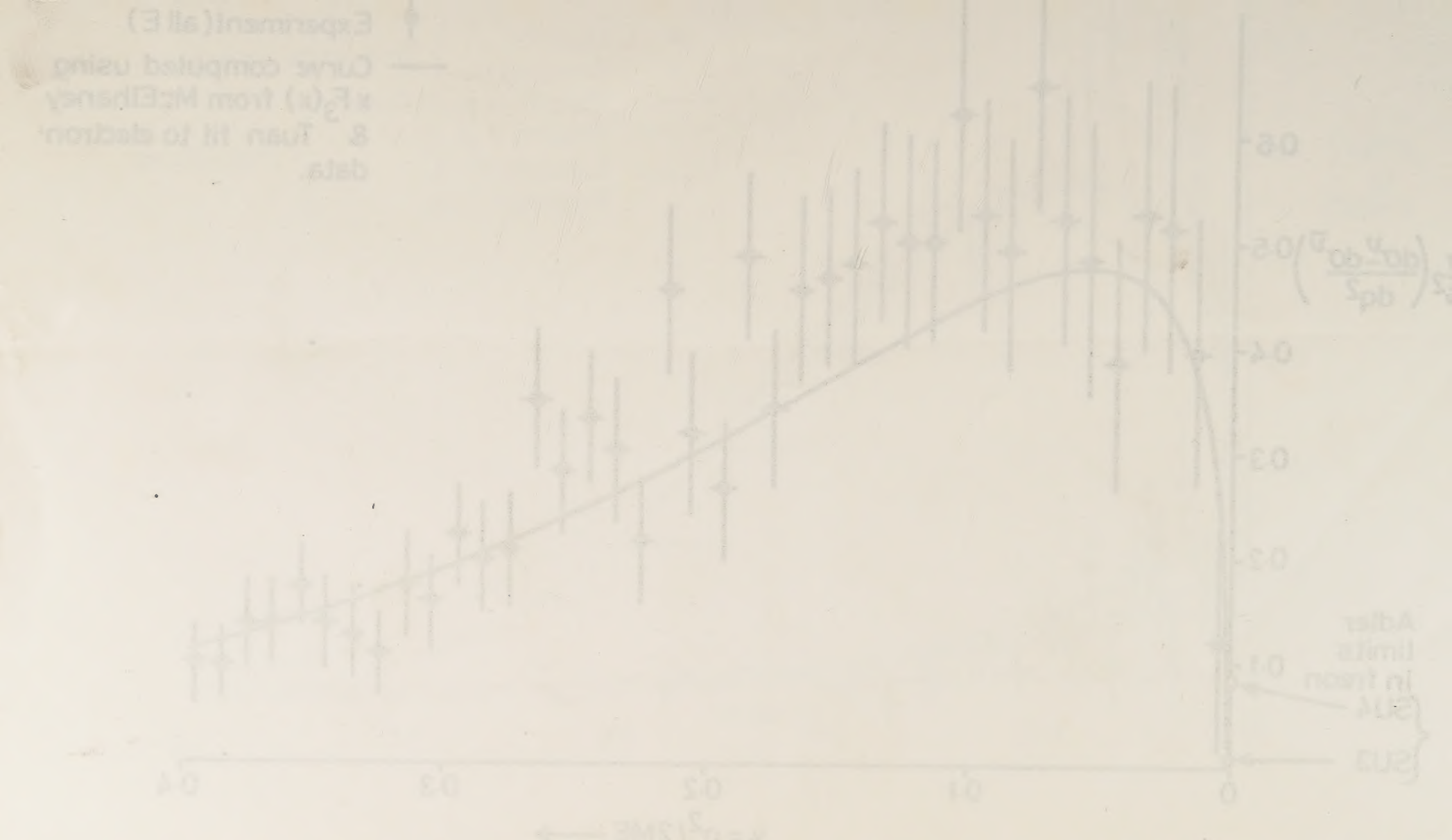
ADLER SUMRULE; DEVIATIONS AT FINITE q^2/E